Manoeuvring coefficients for a wing-model in deep and shallow water

Part I Experiments and test results
Part II Calculations

W. Beukelman

Report 1046-P April 1998

Published in: International Shipbuilding Progress, Volume 45, No. 441, Delft University Press, 1998, P.O. Box 199 2600 AD Delft, The Netherlands

TU Delft

Delft University of Technology

Faculty of Mechanical Engineering and Marine Technology
Ship Hydromechanics Laboratory

International Shipbuilding Progress

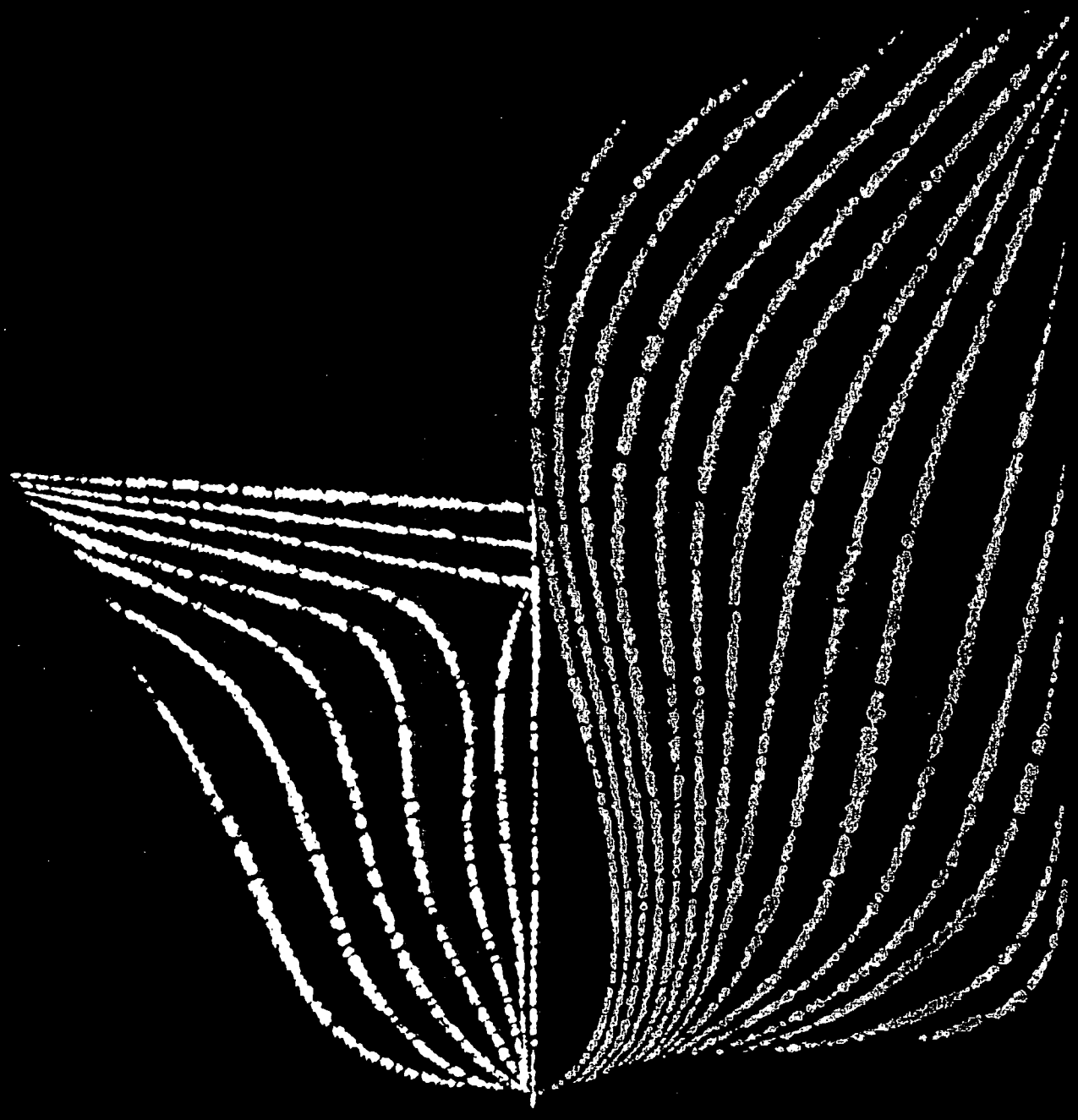

International Shipbuilding Progress

ISSN 0020-868X

Publisher and General Distributor
Delft University Press
Mekelweg 4
2628 CD Delft, The Netherlands
Telephone +31.15.2783254
Telefax +31.15.2781661

Editorial Office
Foundation International Shipbuilding Progress
P.O. Box 199
2600 AD Delft, The Netherlands
Telephone +31.15.2785923
Telefax +31.15.2784264

Rates of subscription 1998
NLG 295.00, excl. 6% VAT per Volume
Orders, and any other business matters, changes of address, claims for the replacement of copies lost in transmission and other enquiries should be addressed to Delft University Press.

Notes to Authors

Publication submitted to ISP should describe scientific work of high international standard, advancing subjects related with the field of Marine Technology in any respect, such as:
- conceptual design,
- structural strength and dynamics,
- hydromechanics and dynamics,
- maritime engineering,
- production of all types of ships,
- production of all other objects intended for marine use,
- shipping science and all directly related subjects,
- offshore engineering in relation to the marine environment,
- ocean engineering subjects in relation to the marine environment.

The contents may be of a pure scientific or of an applied scientific nature dealing with new developments and feasibility aspects.

Written discussions on a paper previously published in ISP, containing significant comments or questions regarding the contents, will be accepted for a period of 6 months following the date of issue of the paper.

All papers and written discussions offered to ISP will be reviewed by at least one member of the board of editors of ISP, in order to decide upon acceptance, rejection or an advice for revision.

Papers submitted should not have been previously published in a generally accessible language, and the author has to confirm that there are no obligations whatsoever which could prevent him from having the paper published in ISP.

The papers should be written in intelligible English and submitted in 3 fold. Line drawings must be submitted as the original, drawn in black india ink on good quality tracing paper, or as a glossary photographic print.
Internationally accepted notations and SI-units (metric), if appropriate, should be used.
It is recommended that the final version of the paper will be made available on a floppy disk as a file of a text editor, prefarably WordPerfect, MS-Word or LaTeX.

INTERNATIONAL SHIPBUILDING PROGRESS

Volume 45, no. 441

Delft University Press / 1998

CONTENTS

MANOEUVRING COEFFICIENTS FOR A WING-MODEL IN DEEP AND SHALLOW WATER

PART I - EXPERIMENTS AND TEST RESULTS

W. Beukelman
Delft University of Technology, Ship Hydromechanics Laboratory, Delft, The Netherlands

Int. Shipbuild. Progr., **45**, no. 441 (1998) pp. 5-50

Received: February 1995
Accepted: May 1996

A model of a surface-piercing wing has been towed through the water at three speeds in two opposite directions for different draughts and drift angles. The experiments were carried out in both deep and shallow water. Purpose of the tests was to measure the longitudinal and transverse forces on the wing-model. From the measured forces hydrostatic manoeuvring coefficients were determined as a function of the drift angle. In addition to these static measurements forced horizontal motion tests with a Planar Motion Mechanism (PMM) were carried out to determine the hydrodynamic manoeuvring coefficients. Calculations based on the potential theory and on the variation of the added mass impulse were carried out to determine the manoeuvring coefficients for small drift angles. Comparison with the measurements showed encouraging results to determine manoeuvring coefficients also for the velocity derivatives.
Both experiments and calculations showed a strong increase of the coefficients with draught and reduction of waterdepth.

Nomenclature

A	connection point of fore oscillator leg to wing model
APP	aft perpendicular
AR	aspect ratio T/L_w
a, b, d, e	hydrodynamic coefficients for seakeeping
a	distance from *LCG* to *CN*

B	beam, connection point of aft oscillator leg to wing model
$b(x)$	local half beam of the wing model
CN	centre where the transverse force acts
D	depth or maximum span of the wing model, drag
FPP	fore perpendicular
$Fn = U/\sqrt{gL_w}$	Froude-number
g	acceleration due to gravity
H	waterdepth
I_{zz}	mass moment of inertia of the wing model with respect to vertical axis through LCG
L	lift force
LCG	length position of centre of gravity
L_w	length of wing model
l	distance between legs of oscillator
m	fluid added mass
m'	sectional added mass
m_w	mass of wing model
mb	maximum beam
N	normal force, moment, potential damping, manoeuvring coefficient
r	radius of curvature of bilge, yaw angle velocity
T	draught of wing model, longitudinal force
U	wing model speed
v	transverse component of model speed U
X	longitudinal force
Y	transverse force, manoeuvring coefficient
x_0, y_0, z_0	represents a system of reference axes fixed in space with origin 0
x, y, z	represent a body fixed system of axes with its origin in LCG
α	phase angle for moments
β	drift angle
ε	phase angle for forces
ψ	yaw angle
ϕ	adjusted phase angle between fore and aft oscillator leg at yaw
ω	circular frequency of oscillation

1. Introduction

For convential ships the directional or course stability may sufficiently be determined from data obtained by full size experiments or forced oscillation tests with a ship model. In this way it is possible to measure the manoeuvring coefficients, which for convential ships in deep water also may be obtained from expressions based partly on

experience and theory [1]. Prediction of a track or manoeuvre on deep water is within some limitations possible.

Up to now it was thought that the determination of manoeuvring coefficients by potential theory mainly fails with respect to the damping coefficient because viscous influence and flow separation can insufficiently be taken into account.

For fast modern ships, such as Ro-Ro ferry boats it is even more difficult to obtain manoeuvring characteristics, especially for particular circumstances such as shallow water, trimmed condition and in waves [2].

As a first step to address this problem it was thought to be useful to design a series of tests with a wing profile model in deep and shallow water to obtain the required experimental data and to compare them with provisional computed poten-tial values.

In the physical model for predicting manoeuvring coefficients the ship is considered to be a wing profile with a very low aspect-ratio.

The calculated transverse force has been determined from the variation of the added-mass impulse, a method proposed by Jones [3] and Payne [4].

The present study is an abbreviated version of a report by Beukelman [5] about manoeuvring derivatives for a low aspect-ratio surface piercing wing-model in deep and shallow water. It is also a follow-up of a report describing the lift production of such a wing-model [6].

The static measurements mentioned there are the same as those considered now, while the calculation method of the transverse force is also simular to the one used to calculate the lift force in the preceding study.

This report, however, only considers the manoeuvring aspects.

To determine the hydrodynamic manoeuvring coefficients forced horizontal motion test with a Planar Motion Mechanism (PMM) were performed in conditions related to the static measurements. A calculation procedure for the coefficients is also presented.

The tests were carried out in a towing tank with a surface-piercing wing-profile model at three speeds in two opposite directions in both deep and shallow water. The longitudinal and tranverse forces on the wing were measured as a function of drift angle for the static measurements and as a function of forward speed at the forced horizontal motions.

These experiments were carried out for three draughts (aspect-ratio's) and four waterdepths including deep water.

Additionally, some tests were performed with faired tips of the bilge instead of the usual square tips to show the viscous influence for the latter condition.

From the measurements of the transverse force and moment the hydrostatic and hydrodynamic manoeuvring coefficients were determined and presented as func-tions of resp. drift angle and forward speed. These results were compared with calculated values for small angles and displacements representing the linear behaviour. The agreement in general appeared to be rather satisfactory.

Similar tests and calculations with a segmented ship model showing also non-linear influences have been performed in the past [7].

2. Model data and test description

The tested model had for each draught a NACA-63_2A-015 wing profile as presented in the book 'Theory of Wing Sections' by Abbot and Doenhoff [8]. The main dimensions and data of the wing model are presented in Table 1.
On the side surface of the wing model lines were drawn in such a way that area's of 5 × 5 cm were obtained with exception of the last stroke at the tail in condition A which has a width of 5.8 cm. In the centre of each area a wire or tuft was attached to show locally the direction of the flow in deep water by photo and video. See Figure 1. The model was situated in the middle of the towing tank which has a width of 4.22 m. At a distance of 1.15 m from the side-wall of the towing tank at a depth equal to the model's actual draught a flow-mill was placed to measure the return flow during the experiments.

Table 1. Main dimensions of NACA-63_2A-015 Wing model.

Length L_W (chord)	2.2577 m
Maximum beam B_{MW}	0.3385 m
Depth (Maximum Span) D	0.500 m
Draught (Actual Span) T	0.10 m (shiplike condition) 0.20 m
	0.30 m, 0.40 (For Fn =.15 and deep water only)
Geometric Aspect-ratio	0.0443, 0.0886
$AR = T/L_W$	0.1329, 0.1772 (For Fn =.15 and deep water only)
Taperratio L_{top}/L_{bottom}	1.0
Sweep angle	0
Centre of gravity in length (LCG) with respect to fore point of wing	0.960 m
Adjusted mass (kg) related to draught (T) and equal to mass of displaced water - m (T)	50.6 kg (T=0.10m) 100.5 kg (T=0.20m) 150.8 kg (T=0.30m) 201.1kg (T=0.40m) (For Fn = .15 and deep water only)
Adjusted mass moment of inertia (kg m^2) with respect to vertical axis through LCG as function of draught (T) - I_{zz} (T)	10.958 kgm^2 (T=0.10m) 23.504 kgm^2 (T=0.20m) 25.424 kgm^2 (T=0.30m) 36.986 kgm^2 (T=0.40m) (For Fn = .15 and deep water only)

For all conditions the experiments were carried out with a model of the wing that

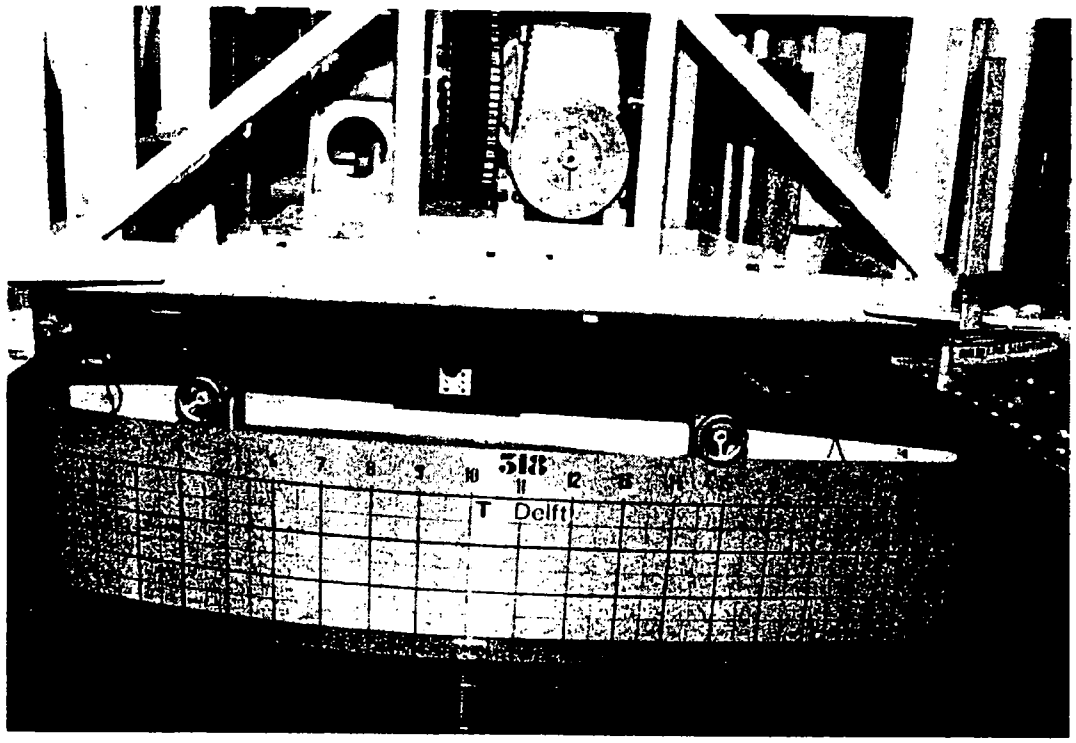

Figure 1. Wing model with PMM under the towing carriage.

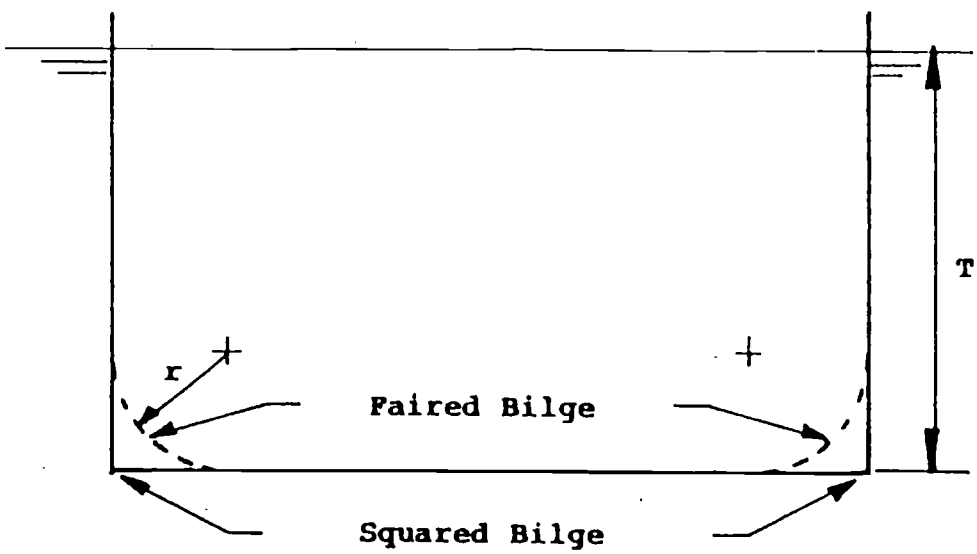

Figure 2. Transverse Wing-Section.

showed a rectangular transverse section, with a hard turn of bilge denoted as *square tips*. See the drawn line of the transverse section in Figure 2. In addition some tests were repeated with a wing model having an easy turn of bilge with a radius of curvature r of 2 cm, denoted as *faired tips*. See the dotted line in Figure 2.

CONDITION A

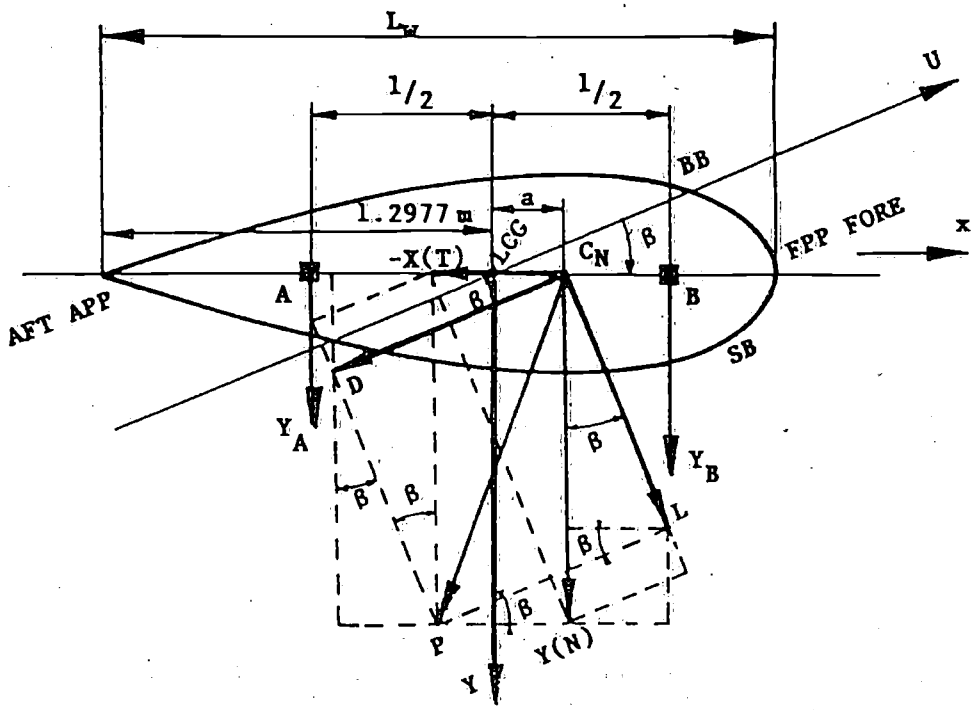

Figure 3a. Forces acting on the wing section for condition A.

CONDITION B

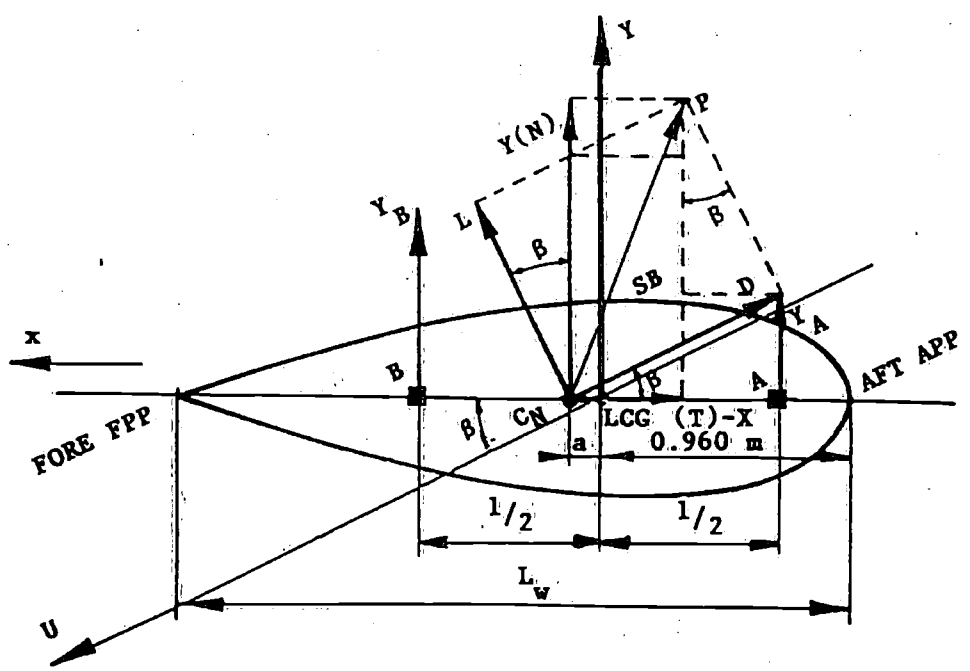

Figure 3b. Forces acting on the wing section for condition B.

For all tests the first measurement with the wing model was performed at forward speed denoted as A-condition in the Tables and Figures. See also Figure 3a. On the way back of the towing carriage the measurement was repeated at the same but reverse speed and position of the wing model. This situation is denoted in the Tables and Figures as the B-condition. See also Figure 3b.
The wing model was attached to two legs of a Planar Motion Mechanism (PMM) by two dynamometers on each leg, one sensitive to the longitudinal direction of the wing model and the other one for the transverse direction. The legs of the oscilla-tor (PMM) were connected to these dynamometers at a distance of 0.5 m fore and aft the Centre of Gravity (*LCG*) of the model and in height at 0.15 m above the base line. The PMM was connected with the towing carriage.

The following conditions for the model with square tips were investigated.
a. *3 draughts* T viz.:
T = 0.10, 0.20 and 0.30 m and in addition T = 0.40 m for Fn = 0.15 and deep water only.
T = 0.10 m approaches the shiplike condition.
According to these tables the draught values agree with the geometric aspect-ratio's $AR = T/L_w$ of 0.0443, 0.0886, 0.1329 with as addition 0.1772 for Fn = 0.15 and deep water only.
The draught T considered was adjusted at zero speed, while at speed the position of the model was kept constant.
b. *3 speeds* forward (A-condition) and back (B-condition) viz.:

Fn	= 0.15	U = 0.706 m/s
	= 0.20	= 0.941 m/s
	= 0.25	= 1.176 m/s

c. *3 waterdepth - draught ratio's H/T* viz.:
H/T = 1.2, 1.6 and 2.0 (shallow water) and for deep water H = 2.50 m and H = 0.60 m for T = 0.10 m.
The waterdepth - draught ratio's are given for the zero speed condition.

The following experiments were carried out with the square tipped model:
a. *Static drift angles*
For drift angle β = 0, 4, 8, 12, 16 and 20 degrees the longitudinal X-force and the transverse Y-force were measured for the denoted draughts, speeds and waterdepth's.
The drift angle β was obtained by rotation of the wing model as denoted for condition A and B in resp. Figure 3a and b.
In these figures U is indicated as the model speed which means that the flow-direction of the fluid should be considered to have the opposite direction.
b. *Horizontal oscillation*
For one low manoeuvring frequency ω = 0.25 rad/s the model was forced to carry out

both the *sway* and *yaw* motion with an amplitude $y_0 = 0.1$ m.
From the measured forces the hydrodynamic manoeuvring coefficients were determined.
Finally, as an *addition*, the static angle test and the horizontal oscillations (sway and yaw) were repeated for the model with *faired tips* related to the condition:

$T = 0.10$ m	$H = 2.20$ m, 0.60 m (deep water)
$T = 0.30$ m	$H = 2.40$ m (deep water)
and	$H = 0.75$ m ($H/T = 2.5$, shallow water)

3. Experiments and test results

The hydrostatic and hydrodynamic manoeuvring coefficients were obtained from the experiments in a way which in general is well known and i.e. presented in [1,9]. Nevertheless the procedure will be described here again because it is a necessary link in view of the relation which will be developed here between the manoeuvring and seakeeping coefficients.
The transverse drift force Y and the moment N as measured during the static drift experiments and the oscillatory motions are presented in a non-dimensional way as follows.

$$Y' = \frac{Y}{\frac{1}{2}\rho U^2 L_w^2} \quad \text{and} \quad N' = \frac{N}{\frac{1}{2}\rho U^2 L_w^3} \tag{3.1}$$

For a review of the way in which each of the measured and calculated coefficients has been made non-dimensional see Table 4-6 (Part II).

3.1. Static measurements

From the total measured sideforce (see Figure 3a and 3b) it follows, that

$$Y_\beta = \frac{Y_A + Y_B}{\beta} \quad \text{and} \quad Y_\beta' = \frac{Y_\beta}{\frac{1}{2}\rho U^2 L_w^2} \tag{3.2}$$

In the same way the total horizontal drift moment on the wing model is found as:

$$N_\beta = \frac{\frac{1}{2}(Y_B - Y_A)}{\beta}) \quad \text{and} \quad N_\beta' = \frac{N_\beta}{\frac{1}{2}\rho U^2 L_w^3} \tag{3.3}$$

The test results for the non-dimensional drift forces Y_β' and the non-dimensional moments N_β' are together with the longitudinal forces $-X$, shown in report [5] as function of the drift angle β for all conditions considered and as an example here for shallow water in the Figures 4 and 5. For deep water see Figures 6 and 7.

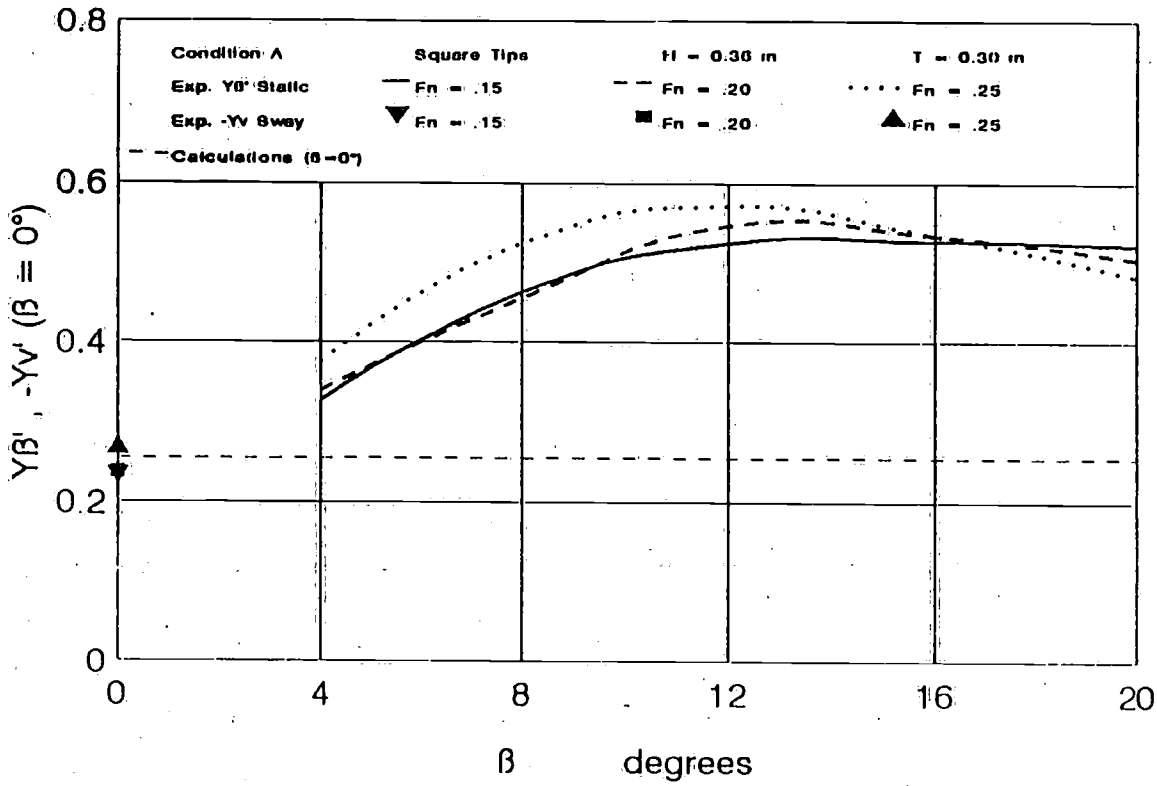

Figure 4. Measurements and calculated values for shallow water, H/T = 1.2.

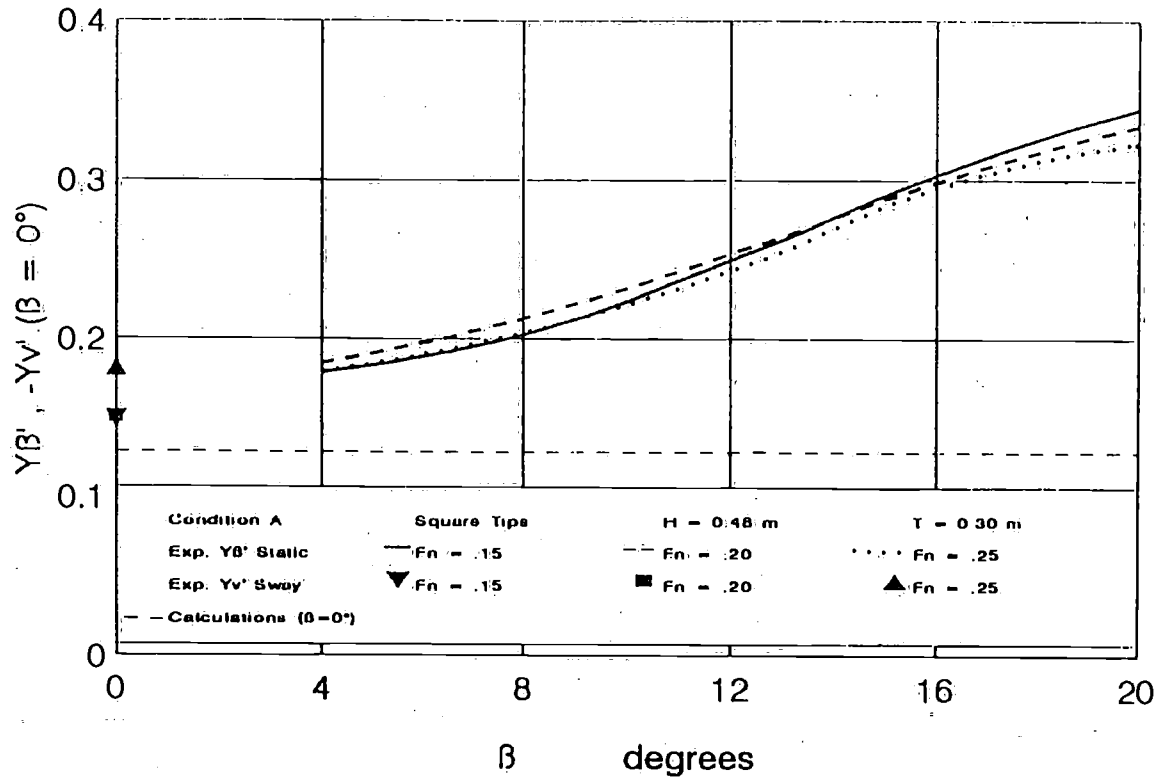

Figure 5. Measurements and calculated values for shallow water, H/T = 1.6.

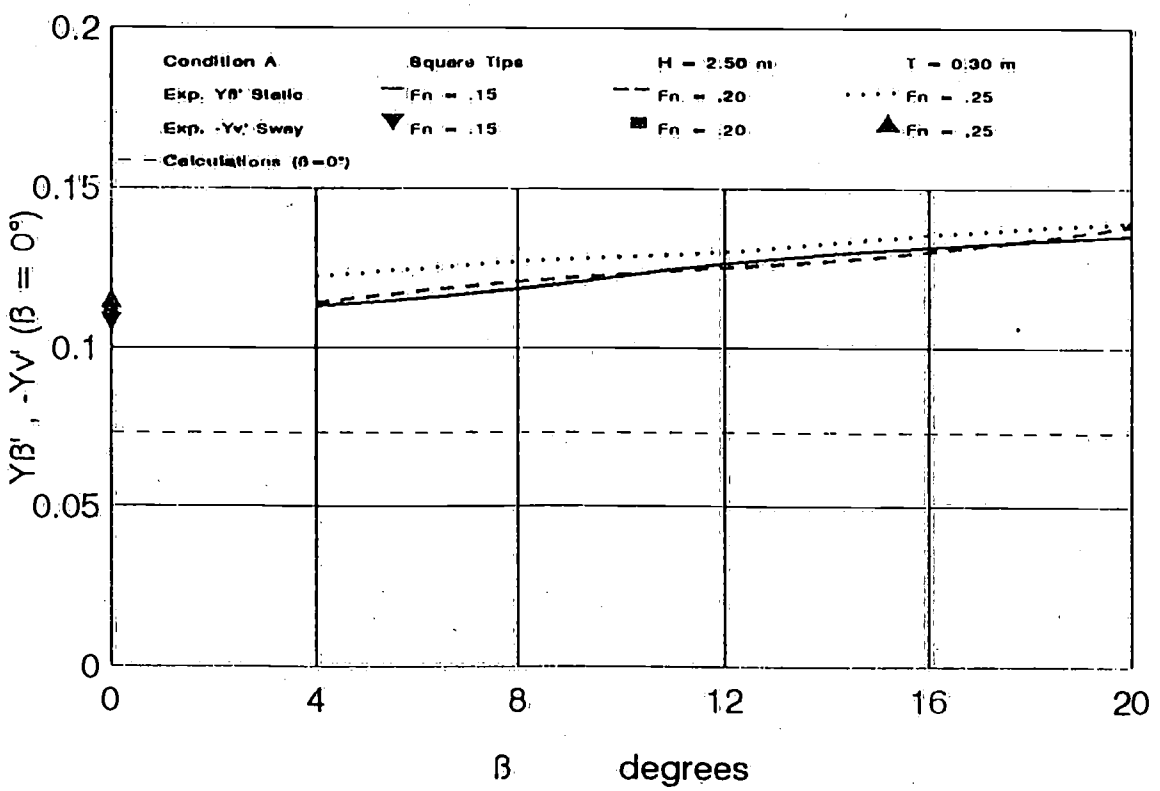

Figure 6. Measurements and calculated values for deep water (square tips of the bilge).

Table 2. Comparison between measured and calculated values for $Y\beta'$ and $N\beta'$, Condition A.

Condition	Measured		Calculated	
	Fn = 0.20, $\beta = 4°$		$\beta = 0°$	
	$Y\beta'$ * 10	$N\beta'$ * 10	$Y\beta'$ * 10	$N\beta'$ * 10
$T = 0.10$ m, $H = 0.12$ m	0.832	0.116	0.780	0.226
Square Tips	0.724*	0.101*		
$T = 0.10$ m, $H = 0.16$ m	0.400	0.079	0.357	0.113
Square Tips	0.448*	0.089*		
$T = 0.10$ m, $H = 0.20$ m	0.325	0.071	0.204	0.076
Square Tips	0.393*	0.086		
$T = 0.10$ m, $H = 0.60$ m	0.247	0.050	0.107	0.043
Square Tips	0.247*	0.050*		
$T = 0.10$ m, $H = 0.60$ m	0.142	0.030	0.107	0.043
Faired Tips	0.142*	0.030*		
$T = 0.10$ m, $H = 2.50$ m	0.197	0.042	0.097	0.040
Square Tips	0.197*	0.042*		
$T = 0.10$ m, $H = 2.20$ m	0.144	0.027	0.097	0.040
Faired Tips	0.144*	0.027*		
$T = 0.30$ m, $H = 0.36$ m	3.390	0.516	2.540	0.923
Square Tips	3.210*	0.489*		
$T = 0.30$ m, $H = 0.48$ m	1.845	0.323	1.275	0.488
Square Tips	1.929*	0.338*		
$T = 0.30$ m, $H = 0.60$ m	1.255	0.245	1.011	0.396
Square Tips	1.303*	0.254*		
$T = 0.30$ m, $H = 0.75$ m	0.930	0.245	1.011	0.396
Faired Tips	0.965*	0.254*		
$T = 0.30$ m, $H = 2.50$ m	1.140	0.248	0.726	0.296
Square Tips	1.140*	0.248*		
$T = 0.30$ m, $H = 2.40$ m	0.855	0.237	0.726	0.296
Faired Tips	0.855*	0.237*		

* Measured values corrected for measured return flow and calculated fall of waterlevel.

Table 3. Comparison between measured and calculated values for Y_β' and N_β', Condition B.

Condition	Measured		Calculated	
	Fn = 0.20, $\beta = 4°$		$\beta = 0°$	
	Y_β' * 10	N_β' * 10	Y_β' * 10	N_β' * 10
$T = 0.10$ m, $H = 0.12$ m	0.914	0.184	0.780	0.236
Square Tips	0.795*	0.160*		
$T = 0.10$ m, $H = 0.16$ m	0.543	0.110	0.357	0.108
Square Tips	0.609*	0.123*		
$T = 0.10$ m, $H = 0.20$ m	0.409	0.090	0.204	0.083
Square Tips	0.495*	0.109*		
$T = 0.10$ m, $H = 0.60$ m	0.235	0.082	0.107	0.053
Square Tips	0.235*	0.082*		
$T = 0.10$ m, $H = 0.60$ m	0.142	0.030	0.107	0.053
Faired Tips	0.142*	0.030*		
$T = 0.10$ m, $H = 2.50$ m	0.184	0.068	0.097	0.050
Square Tips	0.174*	0.064*		
$T = 0.10$ m, $H = 2.20$ m	0.119	0.051	0.097	0.050
Faired Tips	0.119*	0.051*		
$T = 0.30$ m, $H = 0.36$ m	2.506	0.986	2.540	0.989
Square Tips	2.374*	0.934*		
$T = 0.30$ m, $H = 0.48$ m	1.140	0.686	1.275	0.576
Square Tips	1.210*	0.728*		
$T = 0.30$ m, $H = 0.60$ m	0.715	0.518	1.011	0.481
Square Tips	0.742*	0.537*		
$T = 0.30$ m, $H = 0.75$ m	0.543	0.465	0.885	0.437
Faired Tips	0.564*	0.483*		
$T = 0.30$ m, $H = 2.50$ m	0.837	0.487	0.726	0.383
Square Tips	0.869*	0.505*		
$T = 0.30$ m, $H = 2.40$ m	0.700	0.456	0.726	0.383
Faired Tips	0.726*	0.473*		

* Measured values corrected for measured return flow and calculated fall of waterlevel.

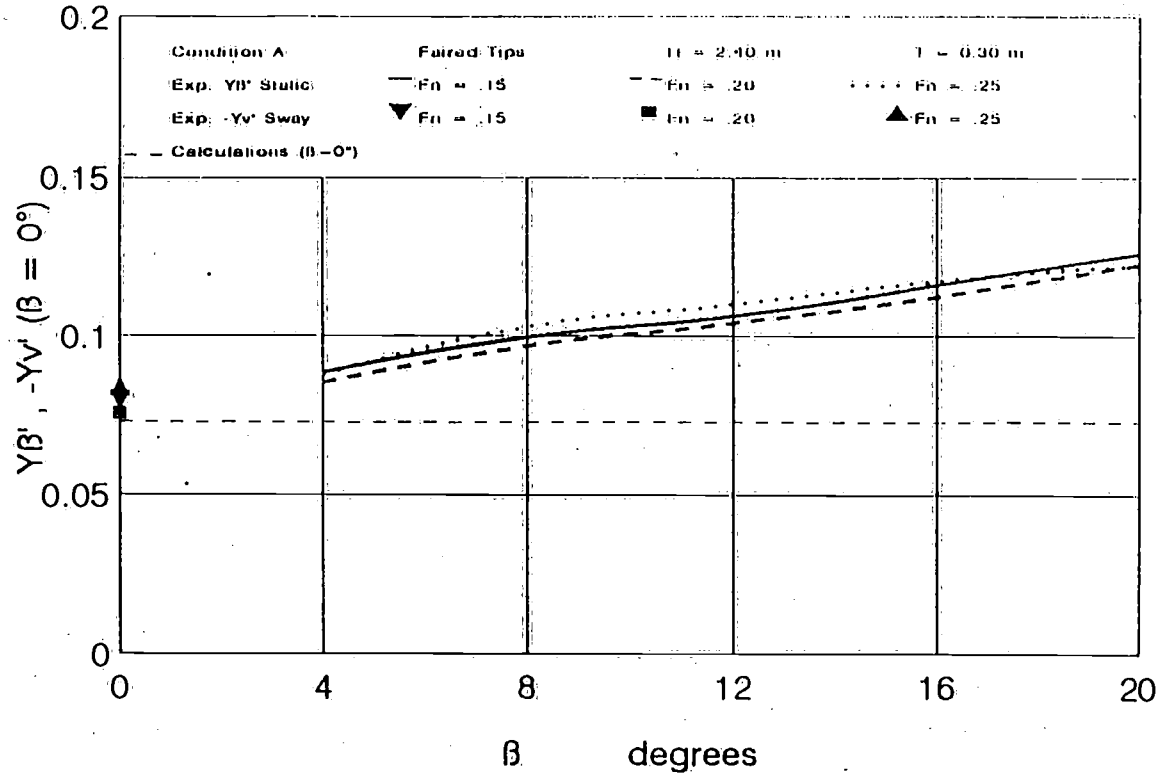

Figure 7. Measurements and calculated values for deep water (faired tips of the bilge).

The experimental values of Y_{β}' and N_{β}' for several conditions are also presented in Table 2 (condition A) and in Table 3 (condition B), for $Fn = 0.20$ and drift angle $\beta = 4°$. The experimental values of Y_{β}' and N_{β}' are also corrected for the measured return flow and calculated fall of waterlevel as presented and discussed in [6]. In these tables the static experimental derivatives Y_{β}' and N_{β}' are also compared with calculated values for $\beta = 0°$ as denoted in section 4.2.2 (Part II).

3.2. Sway oscillation

For this motion the following equations are used (see Figure 3a and b for $\beta = 0$):

$$(Y_{\dot{v}} - m_w)\dot{v} + Y_v v = Y_a \sin(\omega t + \varepsilon) = Y_A + Y_B$$

$$N_{\dot{v}}\dot{v} - N_v v = N_a \sin(\omega t + \alpha) = (Y_B - Y_A)\frac{l}{2} \tag{3.4}$$

in which: m_w - the mass of the wing-model
The transverse displacement of the model is defined as:

$$y = y_a \sin \omega t$$

$$\text{and } v = \dot{y} = \omega y_a \cos \omega t \tag{3.5}$$

$$\dot{v} = \ddot{v} = -\omega^2 y_a \sin \omega t$$

Substitution of (3.5) in (3.4) delivers the hydrodynamic coefficients for sway:

$$Y_{\dot{v}} = \frac{-Y_a \cos \varepsilon}{y_a \omega^2} + m_w$$

$$Y_v = \frac{Y_a \sin \varepsilon}{y_a \omega}$$

$$N_{\dot{v}} = \frac{-N_a \cos \alpha}{y_a \omega^2} \tag{3.6}$$

$$N_v = \frac{N_a \sin \alpha}{y_a \omega}$$

These coefficients for sway in a non-dimensional form $(m_w - Y_{\dot{v}})'$, $-Y_v'$, $-N_v'$ and $-N_{\dot{v}}'$ as function of forward speed are also shown in report [5].
As an example some of these test results for shallow and deep water are presented in the figures 8 and 9.
The relation between the hydrostatic coefficients and the hydrodynamic coefficients for sway may be found with

$$v = -U \sin \beta$$

For small drift angles, so $\beta \rightarrow 0$, it means

$$v = -U\beta \tag{3.7}$$

with $Y_v v = Y_\beta \beta$ it is obvious that

$$Y_\beta' = -Y_v'$$

$$N_\beta' = -N_v' \tag{3.8}$$

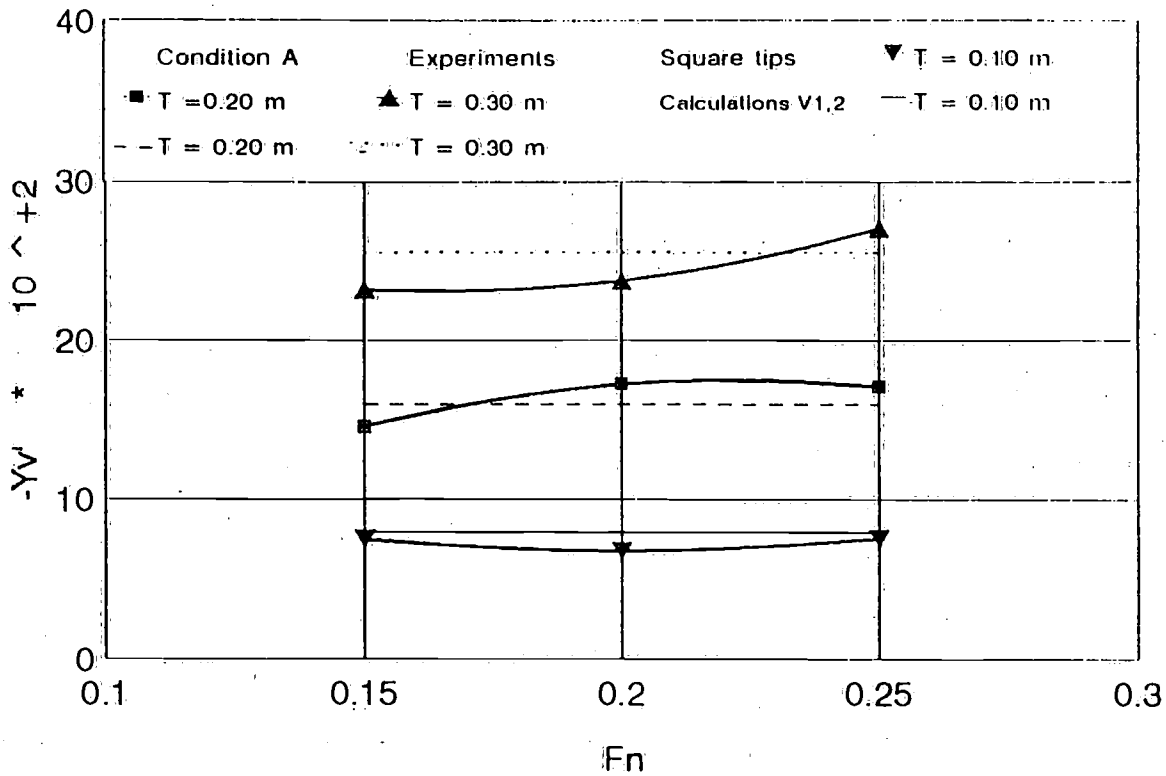

Figure 8. Measured and calculated –Yv' for sway, H/T = 1.2.

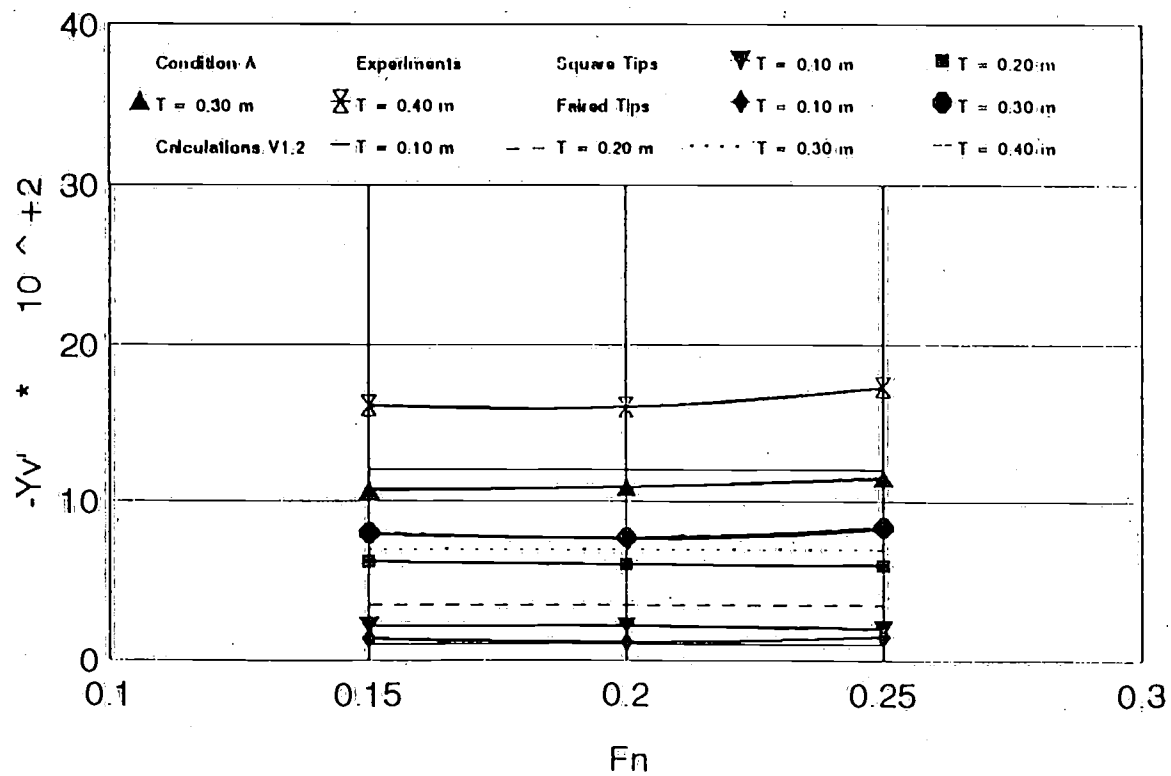

Figure 9. Measured and calculated –Yv' for sway, H = 2.50 m.

3.3. Yaw oscillation

The pure yawing concept in manoeuvring is defined by the absence of a drift angle, hence the velocity vector of *LCG* is tangent to the swaying path of *LCG*. See Figure 3a and b and also Figures 10, 11 and 12. For this case of yawing: $v = \dot{v} = \beta = \dot{\beta} = 0$ while the yawing angle $\psi = \psi_\alpha \cos \psi t$ is considered to be small.
This yawing motion can be split up in a translation of *LCG* (sway) and a rotation (yaw) as shown in Figures 10, 11 and 12 for condition A. If a phase-difference ϕ is introduced between A and B, the displacements of A and B may be defined as:

$$y_A = y_a \sin (\omega t - \frac{\phi}{2}) \tag{3.9}$$

$$y_B = y_a \sin (\omega t + \frac{\phi}{2})$$

The following derivation may be applied to find the phase-angle $\phi/2$:
The transverse speed:

$$U_y = \frac{d}{dt}\left(\frac{y_B + y_A}{2}\right) = \omega y_a \cos\frac{\phi}{2} \cos \omega t \tag{3.10}$$

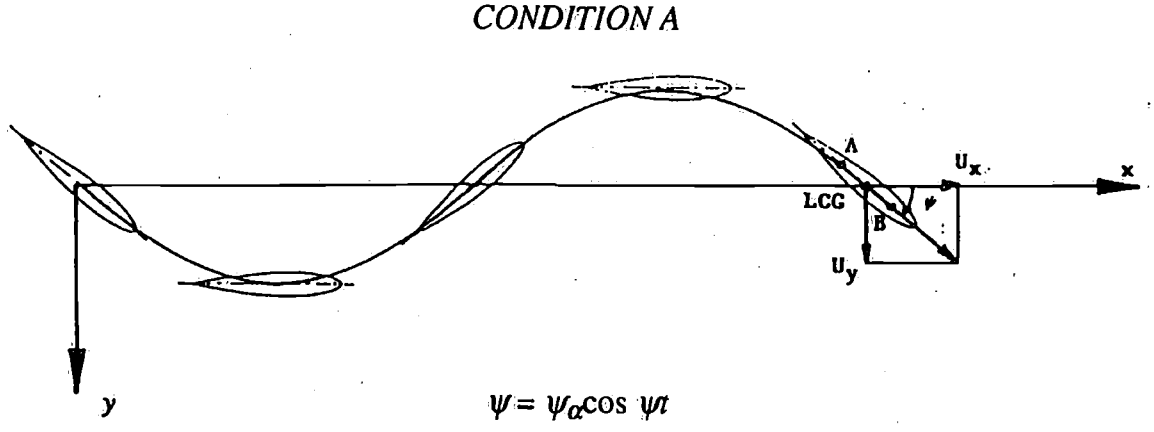

Figure 10. Pure yawing.

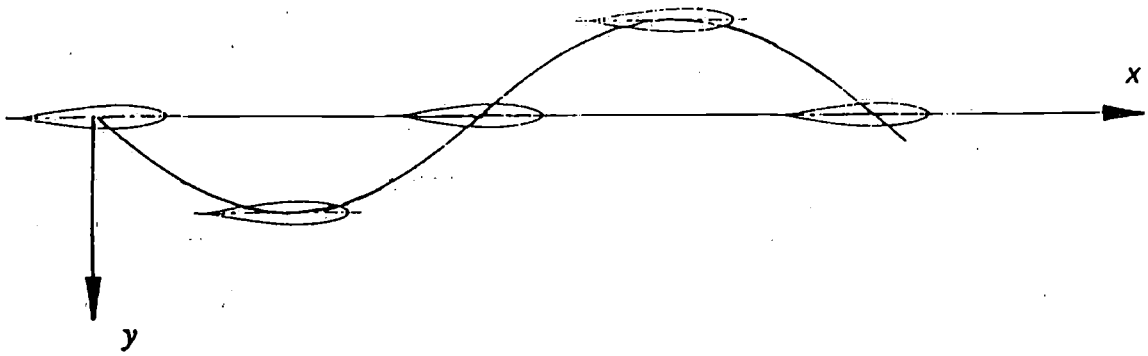

$$y = y_\alpha \sin \psi t$$

Figure 11. Swaying motion ($\psi = \beta = 0$).

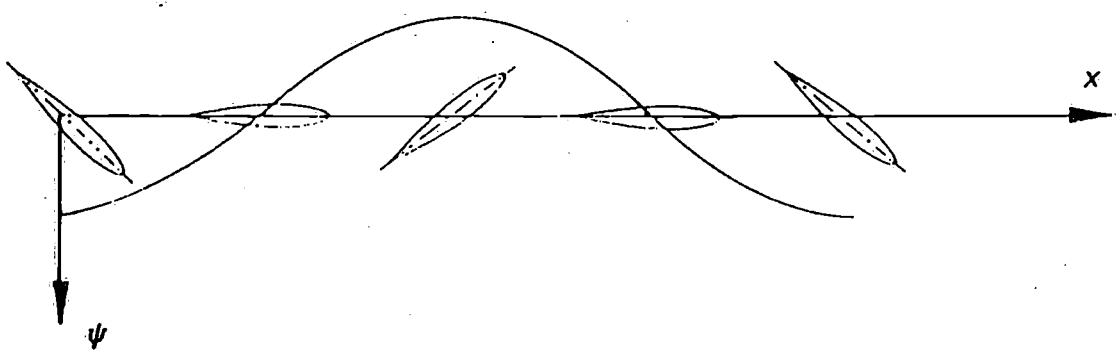

$$\psi = \psi_\alpha \cos \psi t$$

Figure 12. Yawing around z-axis.

The yaw angle for small values is:

$$\psi = \sin \psi = \frac{y_B - y_A}{l} = \frac{2y_a}{l} \sin \frac{\phi}{2} \cos \omega t \tag{3.11}$$

from which follows:

$$\psi_a = \frac{2y_a}{l} \sin \frac{\phi}{2} \tag{3.12}$$

and with

$$\psi = \text{tg } \psi = \frac{U_y}{U_x} = \frac{\sin \psi}{\cos \psi} \tag{3.13}$$

it may be seen that for $\cos \psi \approx 1$:

$$\text{tg}\,\frac{\phi}{2} = \frac{l\omega}{2U_x} \tag{3.14}$$

For each combination of the distance l, the frequency ω and the forward speed of the wing $U \approx U_x$, the phase angle ϕ is adjusted to obtain $v = \dot{v} = \beta = \dot{\beta} = 0$. The equations of the pure yawing motion are

$$(Y_{\dot{r}}\dot{r} + (Y_r - m_w U)r = Y_a \cos(\omega t + \varepsilon)$$

$$(N_{\dot{r}} - I_{zz})\dot{r} + N_r r = N_a \cos(\omega t + \alpha) \tag{3.15}$$

where:
I_{zz} = the mass moment of inertia of the wing with respect to the vertical axis through *LCG*

$N_a = (Y_B - Y_A)\frac{l}{2}$ = the yaw-moment

$$r = \dot{\psi} = -\omega\psi_a \sin \omega t$$

$$\dot{r} = \ddot{\psi} = -\omega^2 \psi_a \cos \omega t \tag{3.16}$$

Substitution of (3.16) into (3.15) delivers the hydrodynamic coefficients for yaw:

$$(Y_r - m_w U) = \frac{Y_a \sin \varepsilon}{\psi_a \omega}$$

$$Y_{\dot{r}} = -\frac{Y_a \cos \varepsilon}{\psi_a \omega^2}$$

$$(N_{\dot{r}} - I_{zz}) = -\frac{N_a \cos \alpha}{\psi_a \omega^2} \tag{3.17}$$

$$N_r = \frac{N_a \sin \alpha}{\psi_a \omega}$$

These hydrodynamic coefficients for yaw in a non-dimensional form $(m_w - Y_r)'$, $-Y_{\dot{r}}'$, $(I_{zz} - N_{\dot{r}})'$, $-N_{\dot{r}}'$ (see Table 5 and 6 presented in part II) are also shown in report [5] as function of forward speed.

As an example some of these test results for shallow and deep water are presented in the figures 13-16. In those figures both conditions A and B are considered.

It should be remarked that for condition B the same phase-angle $\phi/2$ was used as for condition A. This means that there was a counter-phase of 180° and so the desired pure yawing oscillation was not achieved. The consequences of this will be treated in section 4.2.4. For this reason the yaw coefficients for condition B are indicated with a*.

For conclusions, recommendations and references see part II.

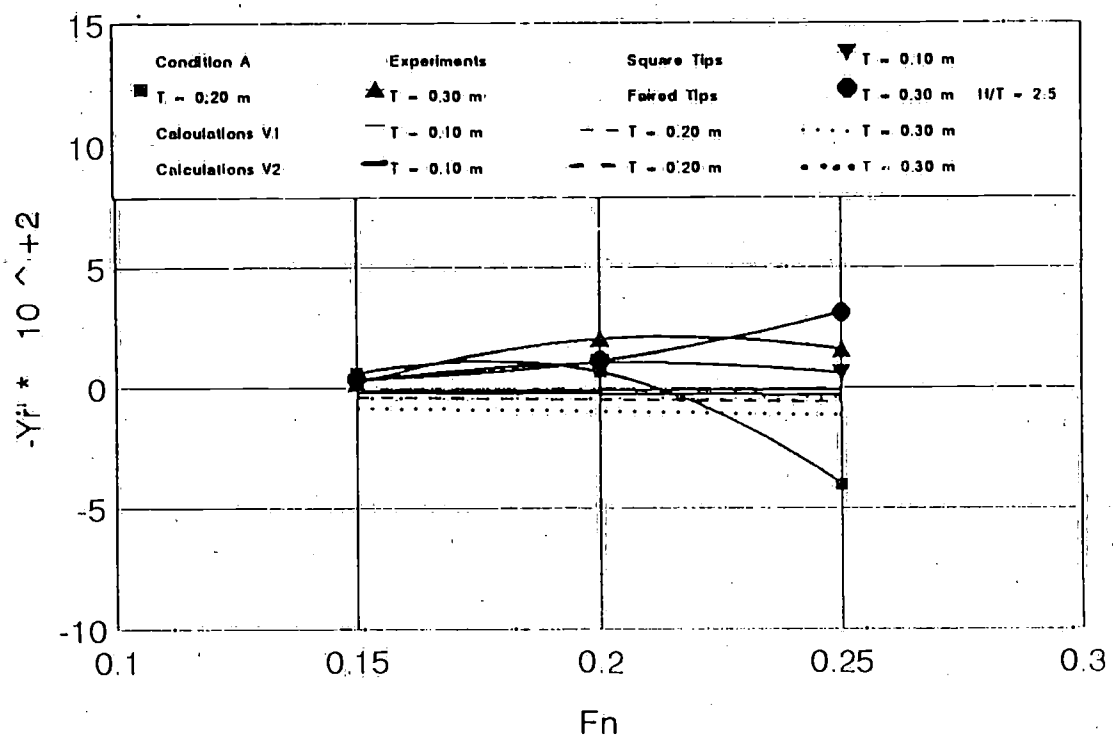

Figure 13. Measured and calculated $-Y\dot{r}'$ for yaw, H/T = 2.0.

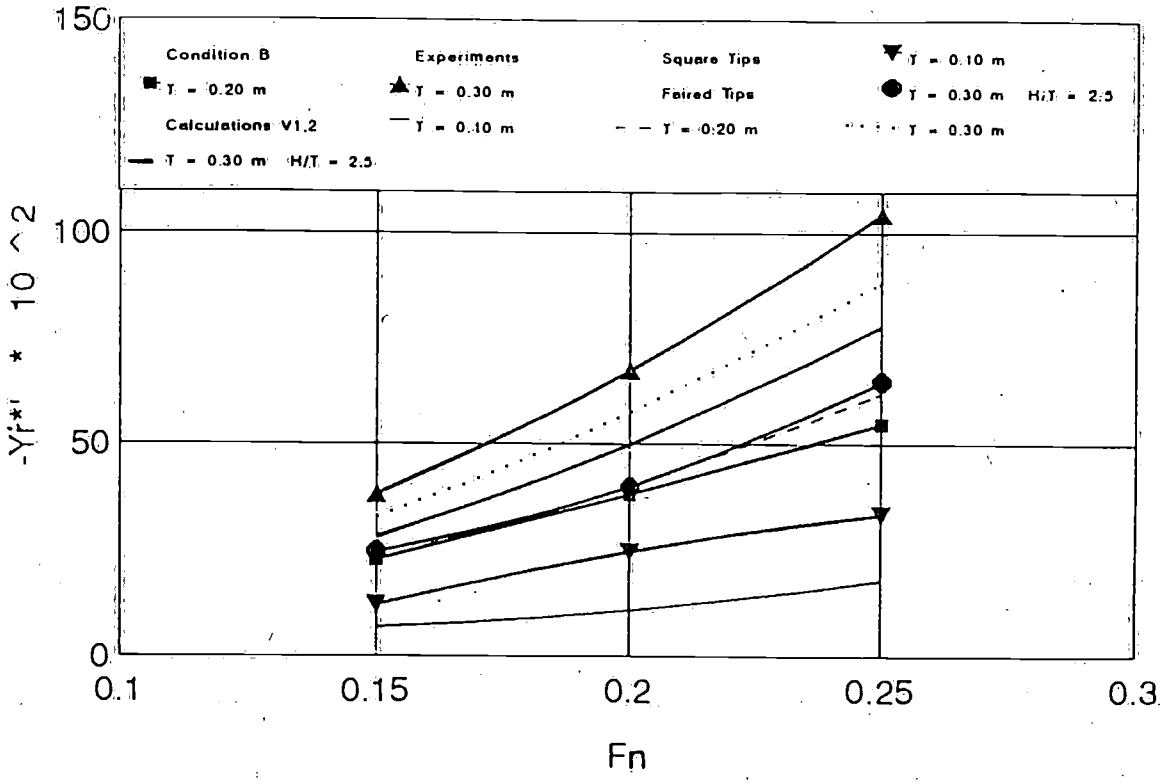

Figure 14. Measured and calculated –Yr' for yaw, H/T = 2.0.*

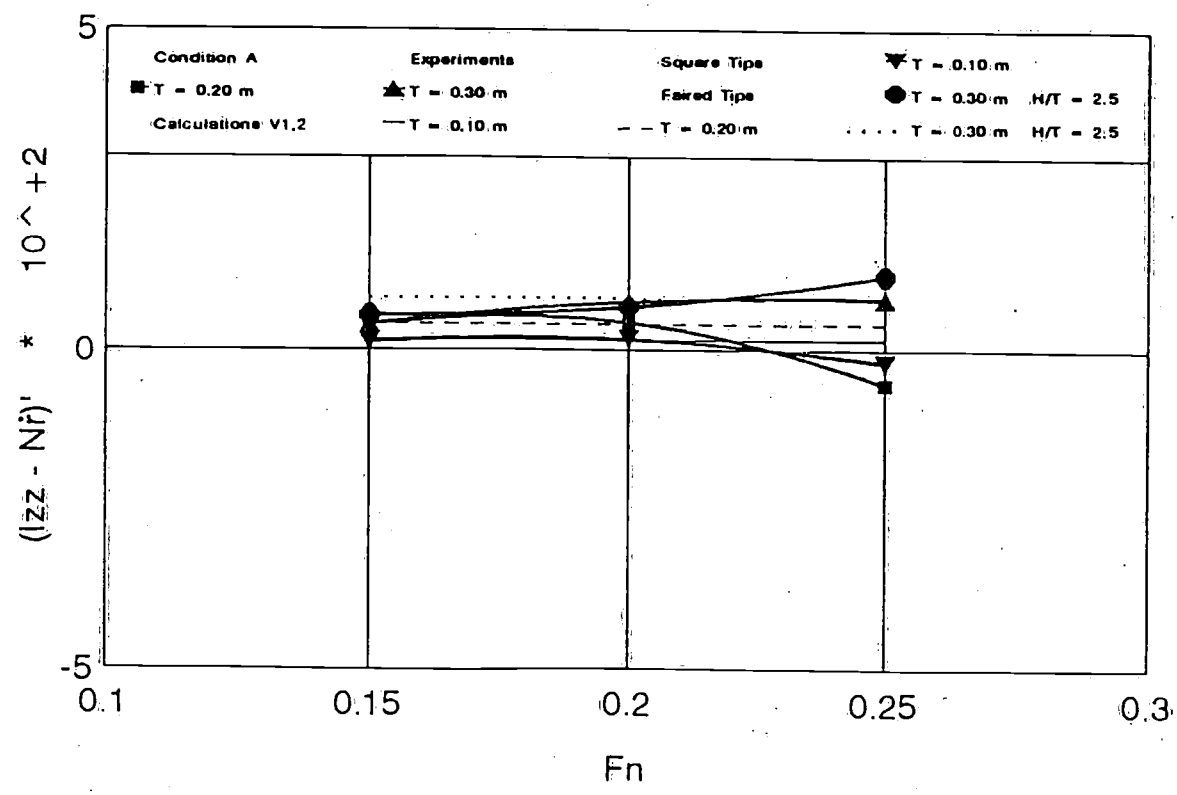

Figure 15. Measured and calculated (I_{zz} - Nr)' for yaw, H/T = 2.0.

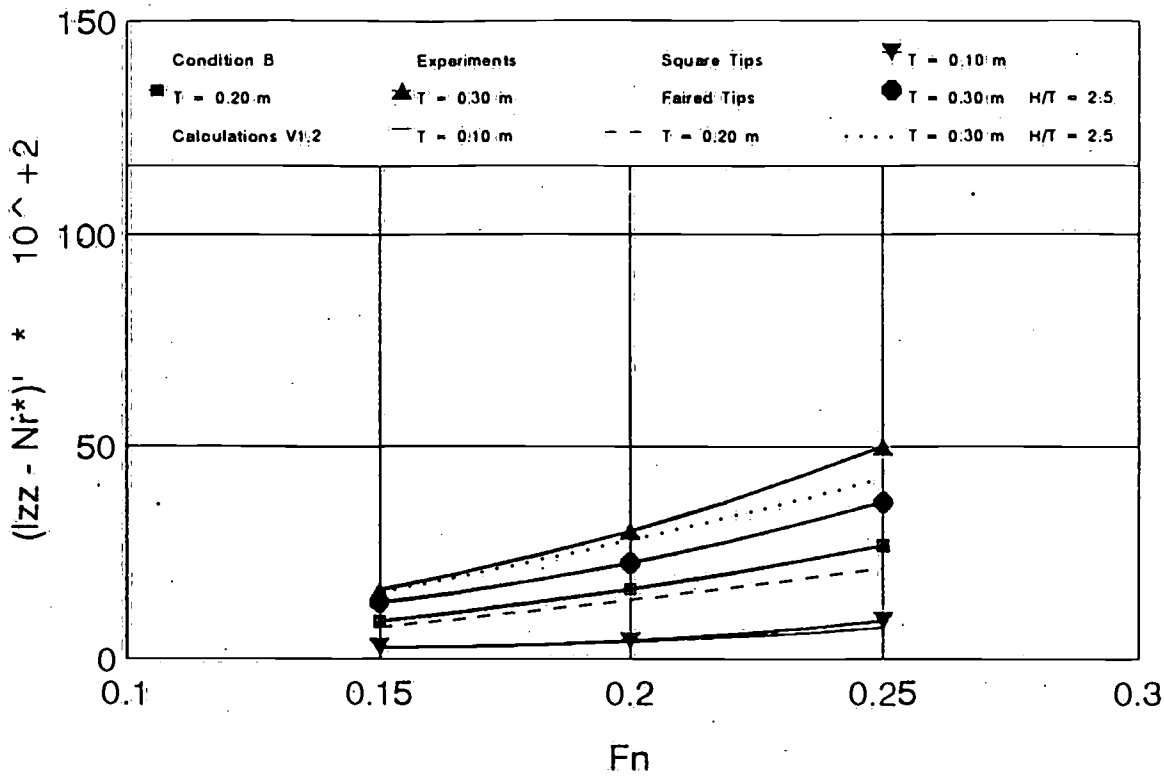

Figure 16. Measured and calculated $(I_{zz} - Nr^*)'$ for yaw, H/T = 2.0.

References

[1] Principles of Naval Architecture, Volume III: Motions in Waves and Controllability, The Society of Naval Architects and Marine Engineers, New York, USA.

[2] Beukelman, W. (1990), The Influence of Trim on the Directional Stability of a Ro-Ro Ship in Shallow Water, Report Nr. 854-E, Ship Hydromechanics Laboratory, Delft University of Technology and presented in Dutch at a Symposium about the Safety of Ro-Ro Ships, Delft University of Technology, The Netherlands.

[3] Jones, R.T. (1945), Properties of Low-Aspect-ratio Pointed Wings at Speeds Below and Above the Speed of Sound, NACA-Report 835.

[4] Payne, P.R. (1992), A Unification in the Added Mass Theory of Planing, Ocean Engineering, Volume 19, No. 1, pp. 39 - 55, United Kingdom.

[5] Beukelman, W. (1995), Manoeuvring Derivatives for a Low Aspect-Ratio Surface Piercing Wing-Model in Deep and Shallow Water, Delft University of Technology, Ship Hydromechanics Laboratory, (MEMT, ISSN 0925-6555, No. 35), ISBN 90-370-0127-0.

[6] Beukelman, W. (1993), Lift and Drag for a Low Aspect-ratio Surface Piercing Wing-Model in Deep and Shallow Water, Delft University of Technology, Ship

Hydromechanics Laboratory (MEMT, ISSN 0925-6555,29), ISBN 90-370-0095-9.

[7] Beukelman, W. (1989), Cross Flow Drag on a Segmented Model, Fourth International Symposium on Practical Design of Ships and Mobile Units (PRADS89), Varna, Bulgaria.

[8] Abbot, Ira H. and von Doenhoff, Albert E. (1958), Theory of Wing Sections, Dover Publications, INC, New York, USA.

[9] Beukelman, W. and Gerritsma, J. (1983), The Longitudinal Distribution of Low Frequency Hydrodynamic Derivatives for Lateral Motions in Shallow Water, Report Nr. 562A, Ship Hydromechanics Laboratory, Delft University of Technology, The Netherlands.

PART II - CALCULATIONS

4. Calculations

4.1. General method

The calculation of the hydrostatic and hydrodynamic manoeuvring coefficients is based upon the potential theory in the same way as described in [6] for the determination of the lift force. For zero drift-angle the transverse force is equal to the lift force (Figure 3a and b). Use has been made of the variation of the added mass impulse method as proposed by Jones [3], Payne [4] and Newman [10].
The determination of added mass and damping is derived for an ideal fluid. This means that this fluid is incompressible, irrotational and inviscid. For such a fluid the Bernoulli equation relates the pressures with the velocities. These flows are characterized as potential flow fields. The flow around the wing is represented by a distribution of sources and sinks only. The equations of motion in the flow are the equivalent of Newtons second law.

The derivative of the local normal or transverse force Y (see Figure 3a and b) may be set equal to the time-derivative of the local added mass impulse in transverse direction and can be written as:

$$\frac{dY}{dx} = \frac{d}{dt}(m'v) \tag{4.1}$$

with m' = the added mass of the fluid per unit length
$v = -U\beta$ = the transverse component of the model speed U (3.7)

Equation (4.1) may be developed into:

$$\frac{dY}{dx} = \frac{dm'}{dt}v + m'\frac{dv}{dt} = \frac{dm'dx}{dx\,dt}v + m'\frac{dvdx}{dxdt} \tag{4.2}$$

Keeping in mind that $dv/dx = 0$ and $dx/dt = -U$ the expression becomes:

$$\frac{dY}{dx} = U^2\beta\frac{dm'}{dx} \tag{4.3}$$

or, also $dY = U^2\beta dm'$ (4.4)

The total transverse or normal force on the wing model will be obtained by integration over the length and so:

$$\int_{APP}^{FPP} dY = U^2\beta \int_{APP}^{FPP} dm' \tag{4.5}$$

$$Y \Big|_{APP}^{FPP} = U^2\beta\, m' \Big|_{APP}^{FPP} = [Y_{FPP} - Y_{APP}] = U^2\beta[m_{FPP}' - m_{APP}'] \tag{4.6}$$

If $m_{FPP}' = m_{APP}' = 0$ which in general is the case the total transverse or normal force will be zero. This phenomenon is quite in accordance with D'Alembert's paradox on the assumption that the flow is irrotational in an ideal fluid without viscosity, vortex sheets and flow separation. Only for a body with a tail fin at the end, so $m_{APP}' \neq 0$ the situation is fundamentally different as stated by Newman in [10]. It is, however, well known that viscosity is required to start the potential lift/ normal force production.
Jones put forward in [3] that with the aid of the Kutta-condition it may be shown easily that sections of the wing behind the section of the greatest width develop no lift.
Katz and Plotkin even showed in [11] that there will be no lift if $b(x)$ is constant with x. Integration up to the section with maximum beam should then be sufficient.
In this way reasonable agreement with the measurements of the lift forces and moments was found in [6], even in the case of restricted waterdepth.
If the integration in eq. (4.6) is carried out from the forward point (*FPP*) to the section with the maximum beam (mb) and if $m_{FPP}' = 0$, it then holds that the transverse force may be written as:

$$Y = U^2\beta\, m_{x_{mb}}' \tag{4.7}$$

The sectional added mass m' was determined using a method based upon potential theory only as denoted before and as presented by Keil in [12] including the influence of restricted waterdepth.
This method has been incorporated by Journée in the computerprogram 'Seaway' as described in [13]. With aid of this computerprogram the hydrostatic and hydrodynamic manoeuvring coefficients were determined based on the expressions derived in the following sections.
The sectional added mass m' may also be obtained by a diffraction method i.e. Delfrac of Pinkster as presented by Dmitrieva in [14]. The advantage of this method is that wall influence or influence of other obstacles in the neighbourhood may be taken into account.

Mikelis and Price (1980) [15] found good agreement with measurements of derivatives in both deep and shallow water through the use of a three-dimensional potential flow analysis of the fluid using a finite element method.
To compute the flow around an arbitrary profile De Koning Gans (1994) [16] developed a higher order three dimensional panel method program. His method has also been applied to determine the pressure distribution around the wing-profile considered here and may also be used to calculate the normal and lift forces.

4.2. Manoeuvring coefficients determined from seakeeping expressions

In the following sections the manoeuvring coefficients will be calculated with aid of the seakeeping coefficients. These coefficients generally are build up from terms with sectional fluid added mass (m') and damping coefficient ($N' - U\,dm'/dx$).
For manoeuvring it is assumed that the oscillation frequency is zero (static measurements) or very low at oscillation so that the damping $N' \rightarrow$ o.
The term $U\,dm'/dx$ of the damping coefficient will deliver the transverse forces as shown in section 4.1. For this reason terms with $U\,dm'/dx$ will be integrated from the forward point (FPP) to the section with the maximum beam (mb). This holds also for terms with m' following from $U\,dm'/dx$ by partial integration. Terms with pure added mass m' will be integrated over the whole modellength Lw as shown experimentally in [9].
Two calculation versions are considered. Version 1 (ordinary strip theory method) is related to the added mass m' only, while version 2 (modified strip theory method) also includes the derivative of the damping N', so

$$(m' + \frac{U}{\omega^2}\frac{dN'}{dx}) \tag{4.8}$$

See for this description also [13, 17].
The other terms with N' remain at zero value, because a very low oscillation frequency is considered (ω = 0.25 rad/s). The derivative of the damping dN'/dx', however, may have a substantial value.
The manoeuvring coefficients are calculated for both versions with the computer-programm 'Seaway' [13].
In the following sections the expressions for the manoeuvering coefficients are determined for version 1 only, but may easily be extended to version 2. For the yawing motion condition A is considered first and secondly condition B, taking into account the counter-phase between fore and aft leg so that the velocity vector of *LCG* was not tangent to the swaying path of *LCG*. See section 3.3 (part I).

4.2.1. Seakeeping expressions

To find the relation between seakeeping and manoeuvring at first the different coordinate systems have to be considered as shown in Figure 17 for condition A.

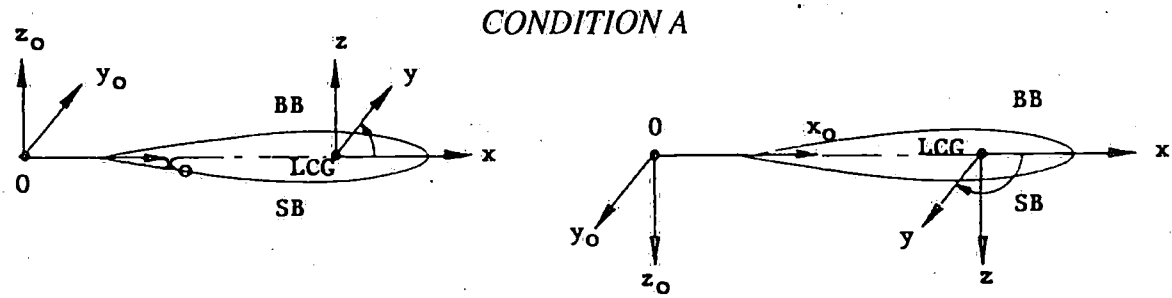

Seakeeping *Manoeuvring*

Figure 17. System of reference axes.

x_0, y_0, z_0 represents a system of reference axes fixed in space with origin O
x, y, z represents a body fixed system of axes with its origin in *LCG*

The most remarkable difference is the choice of the vertical axis z, positive upwards in seakeeping and downwards for manoeuvring. Hence the transverse axis is also different in direction, positive to BB for seakeeping and to SB for manoeuvring.
The equations and notations for seakeeping applied for this case are from [17].
The used equations are for *sway/yaw*

$$(m_w + a_{yy})\ddot{y} + b_{yy}\dot{y} + d_{y\psi}\ddot{\psi} + e_{y\psi}\dot{\psi} = Y_a \sin(\omega t + \varepsilon) \tag{4.9}$$

and for *yaw/sway*

$$(I_{zz} + a_{\psi\psi})\ddot{\psi} + b_{\psi\psi}\dot{\psi} + d_{\psi y}\ddot{y} + e_{\psi y}\dot{y} = N_a \sin(\omega t + \alpha) \tag{4.10}$$

with the sectional values:

$$a'_{yy} = m' + \left[\frac{U}{\omega^2}\frac{dN'}{dx}\right]$$

$$b'_{yy} = N' - U\frac{dm'}{dx}\Big]$$

$$d'_{y\psi} = m'x + [2]\frac{U}{\omega^2}N' - \frac{U^2 dm'}{\omega^2\, dx} + \left[\frac{U}{\omega^2}\frac{dN'}{dx}x\right]$$

$$e'_{y\psi} = N'x - 2U\,m' - U\frac{dm'}{dx}x - \left[\frac{U^2}{\omega^2}\frac{dN'}{dx}\right]$$

$$a'_{\psi\psi} = m'x^2 + 2\frac{U}{\omega^2}N'x - \frac{U^2 dm'}{\omega^2\,dx}x + \left[\frac{U}{\omega^2}\frac{dN'}{dx}dx\right]$$

$$b'_{\psi\psi} = N'x^2 - 2Um'x - U\frac{dm'}{dx}x^2 - \left[\frac{U^2}{\omega^2}\frac{dN'}{dx}x\right]$$

$$d'_{\psi y} = m'x + \left[\frac{U}{\omega^2}\frac{dN'}{dx}x\right]$$

$$e'_{\psi y} = N'x - U\frac{dm'}{dx}x$$

The coefficients in eq. (4.9) and (4.10) are obtained by integration of the sectional values over the model length L_w.

So $a_{yy} = \int_{APP}^{FPP} a'_{yy}dx$ etc.

Version 1 = coefficients excluding terms between brackets
Version 2 = coefficients including terms between brackets

4.2.2. Sway in manoeuvring for conditions A and B

The equation of motion for the swaying motion related to seakeeping with $\psi = 0$ may be written as follows from (4.9):

$$(m_w + a_{yy})\ddot{y} + b_{yy}\dot{y} = Y_a \sin(\omega t + \varepsilon) \qquad (4.12)$$

Substituting $y = y_a \sin \omega t$ delivers for the quadrature component of the side-force:

$$b_{yy}\omega y_a = Y_a \sin \varepsilon \qquad (4.13)$$

The sway oscillation for manoeuvring with also $\psi = 0$ as described in section 3.2 resulted, using eq. (3.6), for the quadrature component of the transverse force in:

$$Y_v\omega y_a = -Y_a \sin \varepsilon \qquad (4.14)$$

The sign for this force is opposite to that found for manoeuvring due to the difference in the direction of the y-axis.
From (4.12), (4.13) and (4.11) it follows that

$$Y_v = -b_{yy} = -\int_{x_{mb}}^{FPP} (N' - U\frac{dm'}{dx})'dx \tag{4.15}$$

and if $N' \rightarrow 0$

$$Y_v = U \int_{x_{mb}}^{FPP} \frac{dm'}{dx} dx$$

with $m'_{FPP} = 0$ this results into

$$Y_v = -Um'_{x_{mb}} \tag{4.16}$$

In non-dimensional form the expressions becomes:

$$Y_v' = \frac{Y_v}{\frac{1}{2}\rho L_w^2 U} = -\frac{m'_{x_{mb}}}{\frac{1}{2}\rho L_w^2} \tag{4.17}$$

In the same way is found for version 1:

$$Y_v = -a_{yy} = -\int_{APP}^{FPP} m'dx \tag{4.18}$$

which becomes in non-dimensional form:

$$Y_v' = -\frac{1}{\frac{1}{2}\rho L_w^3} \int_{APP}^{FPP} m'dx \tag{4.19}$$

The quadrature moment for sway is derived from the yaw/sway equation (4.10) for seakeeping (with $\psi = 0$)

$$e_{\psi y}\omega y_a = N_a \sin\alpha \tag{4.20}$$

and for manoeuvring is found from (3.6)

$$N_v \omega y_a = N_a \sin \alpha \tag{4.21}$$

Combination of (4.20) and (4.21) delivers with (4.11)

$$N_v = -e_{\psi y} = -\int_{x_{mb}}^{FPP} e_{\psi y}' \mathrm{d}x = -\int_{x_{mb}}^{FPP} (N' - U\frac{\mathrm{d}m'}{\mathrm{d}x})x\mathrm{d}x \tag{4.22}$$

and if $N' \rightarrow 0$

$$N_v = U\int_{x_{mb}}^{FPP} \frac{\mathrm{d}m'}{\mathrm{d}x}x\mathrm{d}x \tag{4.23}$$

In non-dimensional form and after partial integration with $m_{FPP}' = 0$ the result is

$$N_v' = -\frac{1}{\frac{1}{2}\rho L_w{}^3}[-x_{mb}m_{x_{mb}}' - \int_{x_{mb}}^{FPP} m'\mathrm{d}x] \tag{4.24}$$

The in-phase relation for sway according to version I results in:

$$-d_{\psi y}\omega^2 y_a = N_v y_a \omega^2$$

and with equation (4.11)

$$N_v = -d_{\psi y} = -\int_{APP}^{FPP} d_{\psi y}'\mathrm{d}x = -\int_{APP}^{FPP} m'x\mathrm{d}x \tag{4.25}$$

The calculated values of $-Y_v'$, $-N_v'$, $(m_w - Y_v)'$ and $-N_v'$ for sway are presented in tables and figures of report [5] and as an example also in the Figure 4 to 9 [part I].

The static coefficients $Y_\beta' = -Y_v'$ and $N_\beta' = -N_v'$ are determined for almost zero frequency of oscillation ($\omega = 0.05$ rad/s). The results are also shown in report [5]. As an example some of the results are also presented in the figures 4 to 9 and in the tables 2 and 3.

4.2.3. Yaw in manoeuvring for condition A

As shown in section 3.3. yaw in manoeuvring may be divided in sway and yaw (Figures 10, 11 and 12) with a mutual phase difference of 90 degrees. The velocity vector of *LCG* is tangent to the swaying path of *LCG*, which is achieved by adjusting a phase angle ϕ between the oscillator legs, so that

$$\text{tg}\,\frac{\phi}{2} = \frac{l\omega}{2U} \tag{3.14}$$

The force equation for sway/yaw follows from equation (4.9) as:

$$(m_w + a_{yy})\ddot{y} + b_{yy}\dot{y} + d_{y\psi}\dot{\psi} + e_{y\psi}\dot{\psi} = -Y_a \sin(\omega t + \varepsilon) \tag{4.26}$$

The force here is taken in phase with the yawing angle ψ and negative in sign in view of the manoeuvring notation. Substitution of $y = y_a \sin \omega t$ and

$$\psi = \psi_a \cos \omega t = \frac{2y_a}{l} \sin \frac{\phi}{2} \cos \omega t \tag{3.11}$$

in (4.26) and using (3.17) and (4.11) yields

$$(Y_r - m_w U) = \frac{Y_a \sin \varepsilon}{\psi_a \omega} = \frac{-\omega^2 (m_w + a_{yy}) y_a - e_{y\psi} \omega \psi_a}{\psi_a \omega}$$

$$\text{or } Y_r = -e_{y\psi} - \frac{\omega (m_w + a_{yy}) l}{2 \sin \frac{\phi}{2}} + m_w U \tag{4.27}$$

$$\text{If } \omega \to 0 \text{ then } \sin \frac{\phi}{2} \to \text{tg}\,\frac{\phi}{2} \to \frac{\phi}{2} \to \frac{l\omega}{2U} \tag{4.28}$$

which results into

$$Y_r = -e_{y\psi} - U a_{yy} \tag{4.29}$$

Substitution of $e'_{y\psi}$ and a'_{yy} as presented in (4.11) and taking $N' \to 0$ for $\omega \to 0$ yields for version 1:

$$Y_r = U \int_{x_{mb}}^{FPP} \frac{dm'}{dx} x dx + 2U \int_{APP}^{FPP} m' dx - U \int_{APP}^{FPP} m' dx$$

$$Y_r = U \left[\int_{x_{mb}}^{FPP} \frac{dm'}{dx} x dx + \int_{APP}^{FPP} m' dx \right] \tag{4.30}$$

In non-dimensional form we find by partial integration

$$Y_r' = \frac{Y_r}{\frac{1}{2}\rho L_w^3 U} = \frac{1}{\frac{1}{2}\rho L_w^3} \left[-x_{mb} m_{x_{mb}}' - \int_{x_{mb}}^{FPP} m' dx + \int_{APP}^{FPP} m' dx \right] \tag{4.31}$$

The in-phase relation of equation (4.26) gives in the same way:

$$Y_r = \frac{Y_a \cos \varepsilon}{\omega^2 \psi_a} = \frac{b_{yy} \omega y_a - d_{y\psi} \omega^2 \psi_a}{\omega^2 \psi_a}$$

$$Y_r = -d_{y\psi} + \frac{b_{yy} l}{2\omega \sin \frac{\phi}{2}}$$

If $\omega \rightarrow 0$ it holds according to (4.28)

$$Y_r = -d_{y\psi} + \frac{b_{yy} U}{\omega^2} \tag{4.32}$$

and with substitution of $d_{y\psi}'$ and b_{yy}' as presented in (4.11) and taking $N' \rightarrow 0$ for $\omega \rightarrow 0$ the result will be for version 1:

$$Y_r = \int_{APP}^{FPP} m' x dx = N_v \tag{4.33}$$

Non-dimensional presentation gives:

$$Y_r' = N_v' = -\frac{1}{\frac{1}{2}\rho L_w^4} \int_{APP}^{FPP} m' x dx \tag{4.34}$$

The moment equation for yaw/sway follows from equation (4.10) and may be transformed for the manoeuvring situation using the same reasoning as for the force equation as follows:

$$(I_{zz} + a_{\psi\psi})\ddot{\psi} + b_{\psi\psi}\dot{\psi} + d_{\psi y}\ddot{y} + e_{\psi y}\dot{y} = -N_a \cos(\omega t + \alpha) \tag{4.35}$$

Substitution of equations (3.11) and (3.17) into equation (4.35) gives for the out-of phase derivative:

$$N_r = \frac{-N_a \sin\alpha}{\omega\psi_a} = \frac{-\omega b_{\psi\psi}\psi_a - \omega^2 y_a d_{\psi y}}{\psi_a \omega}$$

With condition (4.28) this becomes:

$$N_r = -b_{\psi\psi} - U d_{\psi y} \tag{4.36}$$

Substitution of $b_{\psi\psi}'$ and $d_{\psi y}'$ as presented in (4.11) and taking $N' \to 0$ for $\omega \to 0$ results for version 1 in:

$$N_r = U \int_{x_{mb}}^{FPP} \frac{dm'}{dx} x^2 dx + 2U \int_{APP}^{FPP} m' x dx - U \int_{APP}^{FPP} m' x dx$$

$$N_r = U \left[\int_{x_{mb}}^{FPP} \frac{dm'}{dx} x^2 dx + \int_{APP}^{FPP} m' x dx \right] \tag{4.37}$$

After partial integration with $m_{FPP}' = 0$ the non-dimensional presentation becomes:

$$N_r' = \frac{N_r}{\frac{1}{2}\rho L_w^4 U} = \frac{1}{\frac{1}{2}\rho L_w^4} \left[-x^2 m_{x_{mb}}' - 2 \int_{x_{mb}}^{FPP} m' x dx + \int_{APP}^{FPP} m' x dx \right]$$

$$\text{or } N_r' = \frac{1}{\frac{1}{2}\rho L_w^4} \left[-x_{mb}^2 m_{x_{mb}} - 2 \int_{x_{mb}}^{FPP} m' x dx \right] - Y_r' \tag{4.38}$$

The in-phase relation of equation (4.35) delivers in the same way with the manoeuvring equation for yaw (3.17):

$$(N_r - I_{zz}) = \frac{N_a \cos\alpha}{\omega^2 \psi_a} = \frac{-\omega^2 \psi_a (I_{zz} + a_{\psi\psi}) + e_{\psi y} \omega y_a}{\psi_a \omega^2}$$

$$N_r = -a_{\psi\psi} + \frac{e_{\psi y} y_a}{\omega \frac{2y_a}{l} \sin\frac{\phi}{2}}$$

and with condition (4.28) for $\omega \to 0$

$$N_r = -a_{\psi\psi} + \frac{u}{\omega^2} e_{\psi y} \tag{4.39}$$

Substitution of $a_{\psi\psi}'$ and $e_{\psi y}'$ as presented in (4.11) and taking $N' \to 0$ for $\omega \to 0$ results for version 1 in

$$N_r = -\int_{APP}^{FPP} m' x^2 dx \tag{4.40}$$

The non-dimensional presentation is as follows

$$N_r' = \frac{N_r}{\frac{1}{2}\rho L_w^5} = -\frac{1}{\frac{1}{2}\rho L_w^5} \int_{APP}^{FPP} m' x^2 dx \tag{4.41}$$

The expressions for the hydrostatic and hydrodynamic coefficients as put forward here are simular to those presented by Clarke in [18] with the exception of the integration limits in the out-of phase terms for yaw. The calculated values of $(m_w - Y_r)'$, $-Y_r'$, $(I_{zz} - N_r')$ and $-N_r'$ are presented in tables and figures of report [5] and as an example also in the figures 13 and 15 [part I].

4.2.4. Yaw in manoeuvring for condition B

As put forward in section 3.3. for condition B the same phase angle ϕ between the oscillator legs was maintained as for condition A. So there was a counter phase of 180 degrees and a pure yawing oscillation with the velocity vector of *LCG* tangent to the swaying path of *LCG* was not achieved.

The coefficients for condition B are therefore characterized by a*.

At first yawing around the z-axis, being the second component of yawing according to the manoeuvring concept (Figure 12), will be considered. For that case the yaw coefficients could be derived directly from the seakeeping expressions as presented in

(4.11). With $N' \rightarrow 0$ the relations should have been for version 1:

$$Y_r = -e_{y\psi} = U \int_{x_{mb}}^{FPP} \frac{dm'}{dx} x dx + 2U \int_{APP}^{FPP} m' dx \tag{4.42}$$

$$Y_r = -d_{y\psi} = -\int_{APP}^{FPP} m' x dx + \frac{U^2}{\omega^2} \int_{x_{mb}}^{FPP} \frac{dm'}{dx} dx \tag{4.43}$$

$$N_r = -b_{\psi\psi} = U \int_{x_{mb}}^{FPP} \frac{dm'}{dx} x^2 dx + 2U \int_{APP}^{FPP} m' x dx \tag{4.44}$$

$$N_r = -a_{\psi\psi} = -\int_{APP}^{FPP} m' x^2 dx + \frac{U^2}{\omega^2} \int_{x_{mb}}^{FPP} \frac{dm'}{dx} x dx \tag{4.45}$$

Adding a swaying motion, as the first component of yawing according to the manoeuvring concept (Figure 11), is achieved by adjustment of the phase angle ϕ between the oscillator legs as described in 3.3.
This results for Y_r in equation (4.30) in the case of condition A, so

$$Y_r = U \int_{x_{mb}}^{FPP} \frac{dm'}{dx} x dx + 2U \int_{APP}^{FPP} m' dx - U \int_{APP}^{FPP} m' x dx \tag{4.30}$$

Comparison with equation (4.42) shows that the last term,

$$-U \int_{APP}^{FPP} m' dx$$

is added to obtain equation (4.30). This term represents the in-phase part of the swaying component in the out of-phase part of the yawing motion for manoeuvring. This term will have a positive sign in the case of a counter phase of 180° as for condition B and results in:

$$Y_r^* = U \left[\int_{x_{mb}}^{FPP} \frac{dm'}{dx} x dx + 3 \int_{APP}^{FPP} m' dx \right] \tag{4.46}$$

In the non-dimensional presentation this becomes

$$Y_r^{*\prime} = \frac{Y_r^*}{\frac{1}{2}\rho L_w{}^3 U} = \frac{1}{\frac{1}{2}\rho L_w{}^3}\left[\int_{x_{mb}}^{FPP} \frac{dm'}{dx} x\,dx + 3\int_{APP}^{FPP} m'\,dx\right] = N_v' - 3Y_v' \tag{4.47}$$

In the same way it is possible to derive from equations (4.44) and (4.37) for condition B:

$$N_r^{*\prime} = \frac{1}{\frac{1}{2}\rho L_w{}^4}\left[\int_{x_{mb}}^{FPP} \frac{dm'}{dx} x^2\,dx + 3\int_{APP}^{FPP} m'x\,dx\right] = N_r' - 2Y_r' \tag{4.48}$$

Introduction of phase angle ϕ to obtain yaw manoeuvring oscillation, equation (4.43) should be supplied as follows to arrive at Yr for condition A as presented in equation (4.32), so

$$Y_r = -\int_{APP}^{FPP} m'x\,dx + \frac{U^2}{\omega^2}\int_{x_{mb}}^{FPP} \frac{dm'}{dx}\,dx - \frac{U^2}{\omega^2}\int_{x_{mb}}^{FPP} \frac{dm'}{dx}\,dx \tag{4.49}$$

The last term

$$-\frac{U^2}{\omega^2}\int_{x_{mb}}^{FPP} \frac{dm'}{dx}\,dx$$

represents the out-of phase part of the swaying component in the in-phase yawing motion for manoeuvring and is achieved by the phase angle ϕ between the oscillator legs. In case of counter phase of 180° as for condition B the term changes in sign, so

$$Y_r^* = -\int_{APP}^{FPP} m'x\,dx + 2\frac{U^2}{\omega^2}\int_{x_{mb}}^{FPP} \frac{dm'}{dx}\,dx \tag{4.50}$$

In non-dimensional presentation and applying partial integration the expression will be:

$$Y_r^{*\prime} = \frac{Y_r^*}{\frac{1}{2}\rho L_w{}^4} = -\frac{1}{\frac{1}{2}\rho L_w{}^4}\left[-\int_{APP}^{FPP} m'x\,dx - 2\frac{U^2}{\omega^2} m_{x_{mb}}'\right]$$

$$= Y_{\dot{r}}' + 2\frac{U^2}{\omega^2}\frac{1}{L_w{}^2}Y_{\dot{v}}' \tag{4.51}$$

In the same way it is possible to derive from equations (4.45) and (4.39) for condition B:

$$N_{\dot{r}}^{*\prime} = -\frac{1}{\frac{1}{2}\rho L_w{}^5}\left[-\int_{APP}^{FPP} m'x^2\mathrm{d}x + 2\frac{U^2}{\omega^2}\int_{x_{mb}}^{FPP}\frac{\mathrm{d}m'}{\mathrm{d}x}x\mathrm{d}x\right]$$

$$N_{\dot{r}}^{*\prime} = N_{\dot{r}}' + 2\frac{U^2}{\omega^2}\frac{1}{L_w{}^2}N_{\dot{v}}' \tag{4.52}$$

The calculated values of $(m_w - Y_r^*)'$, $-Y_{\dot{r}}^{*\prime}$, $(I_{zz} - N_{\dot{r}}^*)'$ and $-N_r^{*\prime}$ are presented in the tables and figures of report [5] and as an example also in the figures 14 and 16 [part I].

An overview of the above derived expressions for the hydrodynamic manoeuvring coefficients is presented in the Tables 4 - 7.

4.2.5. Overview of manoeuvring coefficients

Table 4. Overview of sway coefficients, condition A and B, version 1

$Y_v = U \int_{x_{mb}}^{FPP} \frac{dm'}{dx} dx$	$Y_v' = \frac{Y_v}{\frac{1}{2}\rho L_w^2 U}$
$= -U m_{x_{mb}}'$	$= \frac{m_{x_{mb}}'}{\frac{1}{2}\rho L_w^2 U}$
$Y_{\dot{v}} = -\int_{APP}^{FPP} m' dx$	$Y_{\dot{v}}' = \frac{Y_{\dot{v}}}{\frac{1}{2}\rho L_w^3}$ $= -\frac{1}{\frac{1}{2}\rho L_w^3}\int_{APP}^{FPP} m' dx$
$N_v = U \int_{x_{mb}}^{FPP} \frac{dm'}{dx} x dx$	$N_v' = \frac{N_v}{\frac{1}{2}\rho L_w^3 U}$
$= U\left[-x_{mb} m_{x_{mb}}' - \int_{x_{mb}}^{FPP} m' dx\right]$	$= \frac{1}{\frac{1}{2}\rho L_w^3}\left[-x_{mb} m_{x_{mb}}' - \int_{x_{mb}}^{FPP} m' dx\right]$
$N_{\dot{v}} = -\int_{APP}^{FPP} m' x dx = Y_{\dot{r}}$	$N_{\dot{v}}' = \frac{N_{\dot{v}}}{\frac{1}{2}\rho L_w^4}$ $= -\frac{1}{\frac{1}{2}\rho L_w^4}\int_{APP}^{FPP} m' x dx = Y_{\dot{r}}'$

Table 5. Overview of yaw coefficients, condition A, version 1.

$Y_r = U[\int_{x_{mb}}^{FPP} \frac{dm'}{dx} x dx + \int_{APP}^{FPP} m' dx]$	$N_r' = \frac{Y_r}{\frac{1}{2}\rho L_w{}^3 U}$
$= -U\,[-x_{mb} m_{x_{mb}}' - \int_{x_{mb}}^{FPP} m' dx + \int_{APP}^{FPP} m' dx]$	$= \frac{1}{\frac{1}{2}\rho L_w{}^3} * [-x_{mb} m_{x_{mb}}' - \int_{x_{mb}}^{FPP} m' dx + \int_{APP}^{FPP} m' dx]$
	$= N_v' - Y_v'$
$Y_\dot{r} = -\int_{APP}^{FPP} m' x dx = N_\dot{v}$	$Y_\dot{r}' = \frac{Y_\dot{v}}{\frac{1}{2}\rho L_w{}^3} = -\frac{1}{\frac{1}{2}\rho L_w{}^4} \int_{APP}^{FPP} m' x dx = N_\dot{v}'$
$N_r = U\,[\int_{x_{mb}}^{FPP} \frac{dm'}{dx} x^2 dx + \int_{APP}^{FPP} m' x dx]$	$N_r' = \frac{N_r}{\frac{1}{2}\rho L_w{}^4 U} = \frac{1}{\frac{1}{2}\rho L_w{}^4} *$
$= U\,[-x_{mb}^2 m_{x_{mb}}' - 2\int_{x_{mb}}^{FPP} m' x dx + \int_{APP}^{FPP} m' x dx]$	$* [-x_{mb}^2 m_{x_{mb}}' - 2\int_{x_{mb}}^{FPP} m' x dx + \int_{APP}^{FPP} m' x dx]$
	$= \frac{1}{\frac{1}{2}\rho L_w{}^4} [-x_{mb}^2 m_{x_{mb}}' - 2\int_{x_{mb}}^{FPP} m' x dx] - Y_\dot{r}'$
$N_\dot{r} = -\int_{APP}^{FPP} m' x^2 dx$	$N_\dot{r}' = \frac{N_\dot{r}}{\frac{1}{2}\rho L_w{}^5} = -\frac{1}{\frac{1}{2}\rho L_w{}^5} \int_{APP}^{FPP} m' x^2 dx$

Table 6. Overview of yaw coefficients, condition B, version 1

$Y_r^* = U\left[\int_{x_{mb}}^{FPP} \frac{dm'}{dx} x\,dx + 3\int_{APP}^{FPP} m'\,dx\right]$	$Y_r^{*\prime} = \frac{Y_r^*}{\frac{1}{2}\rho L_w^3 U} = \frac{1}{\frac{1}{2}\rho L_w^3} * \left[\int_{x_{mb}}^{FPP} \frac{dm'}{dx} x\,dx + 3\int_{APP}^{FPP} m'\,dx\right] = N_v' - 3Y_v'$
$Y_\dot{r}^* = -\int_{APP}^{FPP} m' x\,dx + 2\frac{U^2}{\omega^2}\int_{x_{mb}}^{FPP} \frac{dm'}{dx} dx$ $= -\int_{APP}^{FPP} m' x\,dx - 2\frac{U^2}{\omega^2} m_{x_{mb}}'$	$Y_\dot{r}^{*\prime} = \frac{Y_\dot{r}^*}{\frac{1}{2}\rho L_w^4} = \frac{1}{\frac{1}{2}\rho L_w^4} * * \left[-\int_{APP}^{FPP} m' x\,dx - 2\frac{U^2}{\omega^2} m_{x_{mb}}'\right] = Y_\dot{r}' + 2\frac{U^2}{\omega^2 L_w^2} Y_v'$
$N_r^* = U\left[\int_{x_{mb}}^{FPP} \frac{dm'}{dx} x^2\,dx + 3\int_{APP}^{FPP} m' x\,dx\right]$	$N_r^{*\prime} = \frac{N_r^*}{\frac{1}{2}\rho L_w^4 U} = \frac{1}{\frac{1}{2}\rho L_w^4} * * \left[\int_{x_{mb}}^{FPP} \frac{dm'}{dx} x^2\,dx + 3\int_{APP}^{FPP} m' x\,dx\right] = N_r' - 2Y_r'$
$N_\dot{r}^* = -\int_{APP}^{FPP} m' x^2\,dx + 2\frac{U^2}{\omega^2}\int_{x_{mb}}^{FPP} \frac{dm'}{dx} x\,dx$	$N_\dot{r}^{*\prime} = \frac{N_\dot{r}^*}{\frac{1}{2}\rho L_w^5} = \frac{1}{\frac{1}{2}\rho L_w^5} * \left[-\int_{APP}^{FPP} m' x^2\,dx + 2\frac{U^2}{\omega^2}\int_{x_{mb}}^{FPP} \frac{dm'}{dx} x\,dx\right] = N_\dot{r}' + 2\frac{U^2}{\omega^2 L_w^2} N_v'$

4.3. Semi-empirical methods

In the past several attempts have been made to find empirical expressions for the manoeuvring coefficients at ships based on measured values from planar motion and rotating arm experiments.

Mentioned are here Norrbin (1971) [19], Gerritsma e.a. (1974) [20], Inoue e.a. (1981) [21]. Clarke e.a. (1982) [22] compared several empirical formules against scatter plots of velocity derivatives. Clarke used multiple linear regression analysis to develop empirical formules to explain the variation in the available data for the velocity derivatives and also the acceleration derivatives. His resulting four equations for velocity derivatives were obtained from the pooled data and are, together with the remaining equations for acceleration derivatives, also presented in [1].

Table 7. Comparison of measured, calculated and semi-empirical values for the coefficients.

Condition A $T = 0.10$ m, $H = 2.50$ m									
Manoevring Coefficients	Fn	Experiment		Present calculation		Semi-empirical methods			
		Square Tips	Faired Tips	Version 1	Version 2	Clarke (1982)	Inoue (1981)	Norrbin (1971)	Gerritsma Beukelman Glansdorp (1974)
$-Y_v'$	.15	0.92	0.51	0.89	0.89	0.77	0.90	0.90	0.90
	.20	1.04	0.30						
$*10^2$	.25	1.25	0.62						
$-Y_v'$	.15	2.15	1.39	0.97	0.97	1.17	0.96	1.08	0.96
	.20	2.18	1.18						
$*10^2$	.25	2.02	1.50						
$-N_v'$	.15	–0.11	–0.09	–0.05	–0.06	0.02	–0.05	–0.05	–0.05
	.20	–0.13	–0.05						
$*10^2$	.25	–0.11	–0.17						
$-N_v'$	.15	0.46	0.26	0.40	0.40	0.37	0.39	0.38	0.68
	.20	0.46	0.22						
$*10^2$	.25	0.57	0.28						
$-Y_r'$	.15	–0.05	0.05	–0.05	–0.06	0.04	–0.05	–0.05	–0.05
	.20	0.16	0.12						
$*10^2$	.25	0.12	0.21						
$-Y_r''$	.15	–0.47	–0.31	–0.50	–0.50	–0.27	–0.37	–0.24	–0.24
	.20	–0.38	–0.21						
$*10^2$	.25	–0.66	–0.33						
$-N_r'$	.15	0.01	0.10	0.07	0.07	0.04	0.07	0.07	0.07
	.20	–0.03	0.10						
$*10^2$	.25	–0.07	0.16						
$-N_r'$	.15	0.24	0.14	0.22	0.22	0.18	0.21	0.21	0.15
	.20	0.27	0.16						
$*10^2$	.25	0.27	0.13						

In Table 7 the experimental results of the manoeuvring derivatives for the shiplike

condition T = 0.10 m, H = 2.50 m (deep water) are compared with the present calculation results for version 1 and 2 and the semi-empirical methods mentioned above.
The agreement between experimental, calculated and semi-empirical results appeared to be satisfactory, while the mutual differences between the considered methods are small.

5. Discussion of results

The measured and calculated data in the tables and figures will be compared and discussed now in order of the experiments as described before:

Hydrostatice coefficients
The figures 4 to 7 [part I] present both experimental and calculated results as function of drift angle β together with $-Y_v'$ and $-N_v'$ for $\beta = 0$ from sway experiments and from sway calculations for a very low frequency of oscilla-tion, ω = 0.05 rad/s. These results together with the ones in Table 2 and 3 generally show for condition A and B a good agreement between measure-ments and calculations at $\beta \approx 0°$. This is quite similar as found for the measured and calculated lift forces and moments as presented in [6]. It is also striking that the slope of the derivatives with respect to drift angle β, so $\partial Y_\beta/\partial\beta$ and $\partial N_\beta/\partial\beta$, decreases with increasing waterdepth. This effect might be due to a stronger return flow for restricted waterdepths especially at increasing drift angles.
Furthermore it is clear that in case of faired bilge tips the agreement between experiment and calculation is closer than for square tips. It also appears, that the longitudinal force X, generally somewhat higher for the B-condition, decreases for faired tips and increase of waterdepth, See report [6].
Just as for the lift force, it appears that Y_β' increases strongly with reduction of the waterdepth viz. with a factor 6 à 7 for draught T = 0.10 m as waterdepth H reduces from 2.50 m to 0.12 m. In that case the moment N_β' increases with a factor of about 4 for the same reduction of the waterdepth H.
Moreover it is clear that both coefficients, Y_β' and N_β', grow strongly with draught T or aspect-ratio AR.
The differences between $-Y_v'$ and Y_β', and $-N_v'$ and N_β', for $\beta = 0$ are very small. The corrections for return flow and fall of waterlevel as shown in the tables 2 and 3 demonstrate sometimes remarkable improvements in the comparison with the calculations.

Hydrodynamic coefficients
The measured and calculated hydrodynamic coefficients for sway and yaw are as an

example presented in the figures 8, 9, 13 - 16 (part I). These results are plotted as function of forward speed. See also report [5].

In general the same remarks can be made as for the hydrostatic coefficients. That is, good agreement between experiment and calculation, the best for the model with the faired tips, strong increase with reduction of waterdepth and with increase of the draught T.
The calculated speed influence is found only for the yaw coefficients and N_v' of sway, especially for version 2 and condition B. This is mainly due to the effect of the counter-phase, so that the velocity vector of LCG was not tangent to the swaying path of LCG. This influence clearly demonstrates, that external oscillators, such as a rudder or propeller might change the hydrodynamic coefficients for yaw of the hull prominently. This means that the superposition principle to extend the fixed hull coefficients with external influences of rudder and propeller is quite disputable.
It is hard to tell whether or not version 2 delivers better results for all cases considered. Compared to the measurements it should be remarked that the calculated results according to version 2 show much too high values for shallow water in case of the coefficients N_v' and N_r'. For the future it might be worthwhile to take into account also the small oscillation damping N' and not only the derivative dN'/dx in longitudinal direction. It is striking, that the expression for yaw in condition B shows nice calculated results compared to the measurements.

The results of the semi-emperical methods in Table 7 show for deep water and T = 0.10 m (most shiplike condition) good agreement with the experiments, especially for the faired tips and with the present calculations. It should be stressed that these results are related to the linear part of the manoeuvring coefficients only. For more information about non-linear influences on ship models see [7], where is also indicated that for shallow water conditions the measured manoeuvring coefficients should be corrected for return flow and fall of water level as denoted in [6].

In general it might be clear from this study, that integration of the velocity derivatives up to the maximum beam delivers nice and useful results, which are similar as found for the lift forces in the preceding research [6].
It should, however, be remarked that the comparison of measured and calculated transverse forces here is more direct and therefore better than in report [6], where the lift force composed from transverse force and drag was used for the determination of lift production $\partial L/\partial\beta$. This measured lift slope only could be compared with the calculated one in this report.
Because it was always stated that especially for the velocity derivatives viscous influence should be dominant, observations were made with photo's and video records from the movements of tufts on the underwater hull surface during the runs on deep

water. (See chapter 2 and [6]).
Neither the photo's or the video records show clearly and systematically separation of the flow somewhere along the model except sometimes at the utmost end.
From the comparison between measurements and calculations it is clear that, if the calculated values are considered to represent the potential influence, for faired bilges the viscous damping is rather small. This amounts to an average of 15% from the potential value of the velocity derivatives. For square bilges there is a strong increase of the viscous influence to about 75%. Hence in both cases the potential part in general remains dominant. Especially in shallow water.
In this respect it should be worthwhile to investigate the viscous influence due to the curvature of the bilge and/or the influence of bilge keels.

6. Conclusions and recommendations

The tests with a model of a wing profile in deep and shallow water and the potential theory calculations based upon the variation of the added mass impulse to determine hydrostatic and hydrodynamic manoeuvring coefficients lead to the following conclusions and recommendations:

1. Reduction of waterdepth causes a strong increase of transverse force and moment. Calculated values confirm this very well.
2. Using faired tips at the bilge instead of square tips decreases drag and transverse force considerably and approach rather close the calculated potential values for the latter one.
3. The calculated velocity derivatives are obtained by longitudinal integration of the sectional fluid added mass up to the section with the maximum beam, while acceleration derivatives are found by longitudinal integration over the whole modellength. These results are related to the linear part of the derivatives for zero drift angle.
4. Hydrostatic and dynamic coefficients increase strongly with draught or aspect ratio, but are in general weakly dependent on forward speed. An exception appeared to be the hydrodynamic coefficients for yaw if the velocity vector of *LCG* is not tangent to the swaying path of *LCG*. In that case a strong increase with forward speed may be expected.
5. The presented calculation method supplies a useful tool to determine the manoeuvring coefficients for deep and shallow water showing good agreement with measurements and results of semi-empirical methods for ships in deep water.
6. The greater part of the manoeuvring coefficients is from potential origin, particularly in shallow water.
7. Experiments with a segmented model should be carried out to obtain a better idea

about the longitudinal distribution of the coefficients. During these experiments the measurement of return flow and fall of waterlevel in more detail is essential.

8. The influence of external oscillators, such as a rudder and propeller, on the hull coefficients needs further investigation.
9. Research into viscous influence due to the curvature of the bilge and/or the influence of bilge keels is also needed.
10. The effect of damping due to ship oscillation on manoeuvring should be considered too.

Acknowledgements

The author is highly indebted to the various members of the Ship Hydromechanics Laboratory of the Delft University of Technology for running the wing profile project. Particularly the author wishes to mention mr. A.J. van Strien, who carried out the experiments and a good deal of the calculations. Many thanks also to mr. P.W. de Heer who contributed to the final computations, the design and layout of this report. And last but not least the author is grateful to mr. C.A.M.C. van den Bergh, who manufactured the wing model, took the photo's and made the video records.

References

[1] Principles of Naval Architecture, Volume III: Motions in Waves and Controllability, The Society of Naval Architects and Marine Engineers, New York, USA.

[2] Beukelman, W. (1990), The Influence of Trim on the Directional Stability of a Ro-Ro Ship in Shallow Water, Report Nr. 854-E, Ship Hydromechanics Laboratory, Delft University of Technology and presented in Dutch at a Symposium about the Safety of Ro-Ro Ships, Delft University of Technology, The Netherlands.

[3] Jones, R.T. (1945), Properties of Low-Aspect-ratio Pointed Wings at Speeds Below and Above the Speed of Sound, NACA-Report 835.

[4] Payne, P.R. (1992), A Unification in the Added Mass Theory of Planing, Ocean Engineering, Volume 19, No. 1, pp. 39 - 55, United Kingdom.

[5] Beukelman, W. (1995), Manoeuvring Derivatives for a Low Aspect-Ratio Surface Piercing Wing-Model in Deep and Shallow Water, Delft University of Technology, Ship Hydromechanics Laboratory, (MEMT, ISSN 0925-6555, No. 35), ISBN 90-370-0127-0.

[6] Beukelman, W. (1993), Lift and Drag for a Low Aspect-ratio Surface Piercing Wing-Model in Deep and Shallow Water, Delft University of Technology, Ship

Hydromechanics Laboratory (MEMT, ISSN 0925-6555,29), ISBN 90-370-0095-9.

[7] Beukelman, W. (1989), Cross Flow Drag on a Segmented Model, Fourth International Symposium on Practical Design of Ships and Mobile Units (PRADS89), Varna, Bulgaria.

[8] Abbot, Ira H. and von Doenhoff, Albert E. (1958), Theory of Wing Sections, Dover Publications, INC, New York, USA.

[9] Beukelman, W. and Gerritsma, J. (1983), The Longitudinal Distribution of Low Frequency Hydrodynamic Derivatives for Lateral Motions in Shallow Water, Report Nr. 562A, Ship Hydromechanics Laboratory, Delft University of Technology, The Netherlands.

[10] Newman, J.N. (1977), Marine Hydrodynamics, MIT Press, Cambridge, Massachusetts, USA.

[11] Katz, J. and Plotkin, A. (1991), Low Speed Aerodynamics, from Wing Theory to Panel Methods, McGraw - Hill, International Editions.

[12] Keil, H. (1974), Die Hydrodynamische Kräfte bei der periodische Bewegung zweidimensionaler Körper an der Oberfläche flacher Gewasser, Institut für Schiffbau der Universität Hamburg, Bericht No. 305.

[13] Journée, J.M.J. (1992), Seaway - Delft, User Manual of Release 4.00, DUT/DSL Report No. 910, Ship Hydromechanics Laboratory, Delft University of Technology, The Netherlands.

[14] Dmitrieva, Dr. I. Numerical Investigations of Motions and Drift Forces on Different Bodies Using the DELFRAC Program, Report 1016, Ship Hydromechanics Laboratory, Delft University of Technology, The Netherlands.

[15] Mikelis, N.E. and Price, W.G. (1980), Comparisons of Acceleration Coefficients and Correction Factors Associated Between Theory and Experiments, Transactions RINA, 1980.

[16] Koning Gans, H.J. de (1994), Numerical Time dependent Sheet Cavitation Simulations using a Higher Order Panel Method, Ph.D.Thesis, Delft University Press, ISBN 90-6275-965-3, The Netherlands.

[17] Beukelman, W. and Gerritsma, J. (1982), The Distribution of Hydrodynamic Mass and Damping of an Oscillating Shipform in Shallow Water, Eleventh Scientific and Methodological Seminar on Ship Hydrodynamics, Bulgarian Ship Hydromechanics Centre, Varna, Bulgaria. Report No. 546, Ship Hydromechanics Laboratory, Delft University of Technology, The Netherlands.

[18] Clarke, D. (1972), A Two-Dimensional Strip Method for Surface Ship Hull Derivatives: Comparison on Theory with Experiments on a Segmented Tanker Model, International Symposium on Directional Stability and Control of Bodies Moving in Water. The Institution of Mechanical Engineers, London, United Kingdom.

[19] Norrbin, N.H. (1971), Theory and Observations on the Use of a Mathematical

Model for Ship Manoeuvring in Deep and Confined Waters, Swedisch State Shipbuilding Experimental Towing Tank, Publ. 68, 1971.

[20] Gerritsma, J., Beukelman, W. and Glansdorp, C.C., (1974), The Effect of Beam on the Hydrodynamic Characteristics of Ship Hulls, 10th Office of Naval Research Symposium, Boston, USA or Report No. 403-P, Ship Hydromechanics Laboratory, Delft University of Technology, The Netherlands.

[21] Inoue, S., Hirano, M. and Kijima, K. (1981), Hydrodynamic Derivatives on Ship Manoeuvring, International Shipbuilding Progress, Volume 28, No. 321, May 1981, Rotterdam, The Netherlands.

[22] Clarke, D., Gedling, P. and Hine, G. (1982), The Application of manoeuvring Criteria in Hull Design Using Linear Theory, Transactions RINA, 1982.